

Table 1. Performance of normal, fresh frozen, and FFPE samples on Affymetrix GeneChip Mapping 10K v2, 50K Xba, 250K Nsp, and 250K Sty arrays

Type	Array	PCR yield* (μ g)	Call rate [†] (%)	AA call (%)	AB call (%)	BB call (%)	Signal detection [‡] (%)	MCR [§] (%)	MDR (%)	Overall concordance [¶] (%)
Fresh tumor	10K v2	20.4	93.44	37.96	23.50	38.54	99.82	—	—	96.20
FFPE tumor	10K v2	19.2	86.30	39.77	19.83	40.41	97.39	—	—	—
Fresh tumor	50K Xba	48.3	90.07	40.28	20.24	39.48	—	87.65	98.57	56.95
FFPE tumor	50K Xba	46.0	31.86	47.30	6.76	45.94	—	15.25	22.15	—
Normal	250K Nsp	115.1	95.86	37.95	25.54	36.51	—	94.22	98.60	—
Fresh tumor	250K Nsp	114.4	93.99	41.81	18.09	40.10	—	88.26	98.52	94.74
FFPE tumor	250K Nsp	71.6	79.84	43.42	14.89	41.69	—	65.60	80.32	—
Normal	250K Sty	121.1	93.05	38.87	24.28	36.85	—	90.90	97.45	—
Fresh tumor	250K Sty	114.4	92.96	42.38	17.59	40.03	—	87.95	98.38	92.07
FFPE tumor	250K Sty	95.4	75.17	43.66	16.68	39.66	—	62.57	79.37	—

*For the 250K arrays, this is the total yield of DNA obtained after combining three PCRs according to protocol. For the 10K v2 and 50K arrays, the PCR yield for the FFPE tissues was increased by increasing either the number of reactions or the number of PCR cycles.

[†]Percentage of SNPs able to be genotyped.

[‡]Signal detection used to assess 10K arrays.

[§]Modified partitioning around medoids (MPAM; a genotyping algorithm; ref. 17) call rate used to assess 100K and 500K arrays.

^{||}MPAM detection rate used to assess 100K and 500K arrays.

[¶]Percentage of SNPs genotyped in both fresh frozen and FFPE samples that are given the same genotype.

platform. Importantly, it indicates the need to exclude SNPs on larger fragments for reliable genotype data. Because SNP fragment size is distributed randomly across the genome, the general effect of excluding larger fragment sizes is to reduce the overall resolution without preferentially losing extensive coverage in specific regions (see Supplementary Fig. S1). The effect of fragment size on concordance was specific to FFPE samples and is not observed in comparisons between frozen samples (data not shown).

LOH and copy number assessment. The reliability of genotype assignments using paraffin samples suggests their suitability for LOH predictions. In fact, FFPE and fresh tumor pairs produced similar LOH profiles when including SNPs on fragments sizes ≤ 700 bp (Fig. 2A). Regions of inconsistent LOH predictions between paired samples (for example, see Fig. 2A, boxes) were predicted independently by both Nsp and Sty arrays and appeared along concentrated regions, rather than being sporadically distributed across the genome, suggesting that they reflected true biological differences between the samples. We assessed several discordant regions of LOH using conventional microsatellite marker analysis and in all cases, the microsatellite analysis confirmed that the array predictions were genuine (data not shown).

The ability to associate copy number estimates with SNP genotypes relies on quantitation of SNP probe intensities (14). Because larger fragment SNPs were inadequately amplified during WGS, these SNPs were noninformative for copy number analysis of FFPE samples (Supplementary Fig. S2A). Exclusion of these large fragment SNPs significantly increased the amplitude (signal) of copy number shifts and at the same time reduced the SD (noise) associated with the copy number estimates for all FFPE samples but not the fresh frozen samples (Supplementary Fig. S2B). This increase in signal to noise ratio justifies the use of such a filter, which maintained 308,788 SNPs for FFPE copy number analysis (Table 2). Probe intensities from the remaining smaller fragment SNPs predicted copy number profiles for FFPE samples consistent with those from matching fresh frozen material (Fig. 2B).

Equivalent copy number changes were predicted between FFPE and fresh frozen pairs both across different chromosomes and different sample sets (Fig. 2C).

In addition to limiting fragment size, compensation against fragment size bias was necessary to produce reliable copy number predictions. Although bias due to amplicon size can be negligible when using high-quality DNA, it becomes exaggerated when the DNA sample is degraded (Fig. 3, top). For FFPE samples, the mean copy number was grossly affected by the size of the amplicon carrying the SNP, such that smaller amplicons SNPs predicted gains and larger amplicons SNPs predicted losses in copy number. Quadratic regression helped to neutralize this fluctuation in mean copy number (Fig. 3, middle). Exclusion of SNPs on amplicons > 700 bp before regression effectively removed the fragment size bias from copy number detection (Fig. 3, bottom). Copy number analysis of FFPE samples was done using the freely available CNAG_v2.0 software¹² (15), which automatically uses compensation against fragment size bias and includes an option to exclude SNPs based on fragment size. Alternate software tools that lack this compensation produced copy number estimates from FFPE samples that were noisier even with exclusion of large fragment sizes (data not shown).

Comparison of Mapping 10K, 100K, and 500K array performance. Although the various Mapping arrays all use the same technology and similar assays for genotype and copy number analysis, they each have differences that may influence their compatibility with FFPE samples. Particularly, the Mapping 500K and 10K arrays share the same amplicon distribution during the PCR step of WGS, but the Mapping 100K assay relies on a wider amplicon size distribution (250–2,000 bp). Consequently, Mapping 100K data are more significantly affected by DNA degradation; for example, there are only 59 SNPs on fragment sizes < 500 bp on the Mapping 50K Hind array. Previously, we showed the application of FFPE DNA to the 10K arrays (3) although without the analytic tools applied here. Now, we compared performance of FFPE samples on all Mapping arrays. As expected, call rates and concordances were

poor when FFPE DNA was applied to the Mapping 100K assay, whereas performance was similar for the Mapping 500K and 10K arrays (Table 1; Supplementary Fig. S3). Furthermore, both the Mapping 500K and the 10K arrays, but not the Mapping 100K arrays, provided correct copy number predictions from FFPE DNA, whereas the Mapping 500K arrays best accommodated SNP filters to retain high genomic resolution (Supplementary Fig. S3).

Prediction of mapping array performance for a range of FFPE samples. DNA from FFPE samples can vary in quality as a result of the fixation protocol, years of storage, the extraction protocol, tissue source, and several other uncontrollable and controllable variables. To both identify a method for qualifying FFPE DNA samples for array analysis and test our guidelines for FFPE DNA extraction and data analysis, we measured the performance of an additional 25 FFPE tissue sources processed at separate institutes and stored for 1 to 17 years (Supplementary Table S1). These samples were not prescreened nor selected based on expected performance. Experiments were done without

matched fresh frozen or nontumor samples. In a small test set, we found that application of 90 µg PCR product from FFPE samples increased call rates by several percentage points (data not shown); therefore, we assayed these samples using 90 µg whenever possible, even if this required pooling extra PCRs.

For each sample, we noted the largest amplicon size produced during RAPD-PCR as well as the size range of PCR products during the Mapping assay. Call rates were calculated for SNPs on fragment size ≤200 bp, 250 bp, 300 bp, and so on to determine the size at which call rates dropped <90%. This call rate drop-off value was used to indicate genotyping efficiency and reliability because fragment sizes with high call rates provided high concordance as well. Call rate drop-off values ranged from 250 to 750 bp compared with 700 to 850 bp for the five FFPE ovarian tumors. Therefore, most of these samples would provide reduced resolution for genotype and LOH. Copy number detection was more robust than genotype, and those cutoffs ranged from 300 bp up to no filter requirement at all. Plots of copy number versus fragment size were evaluated to

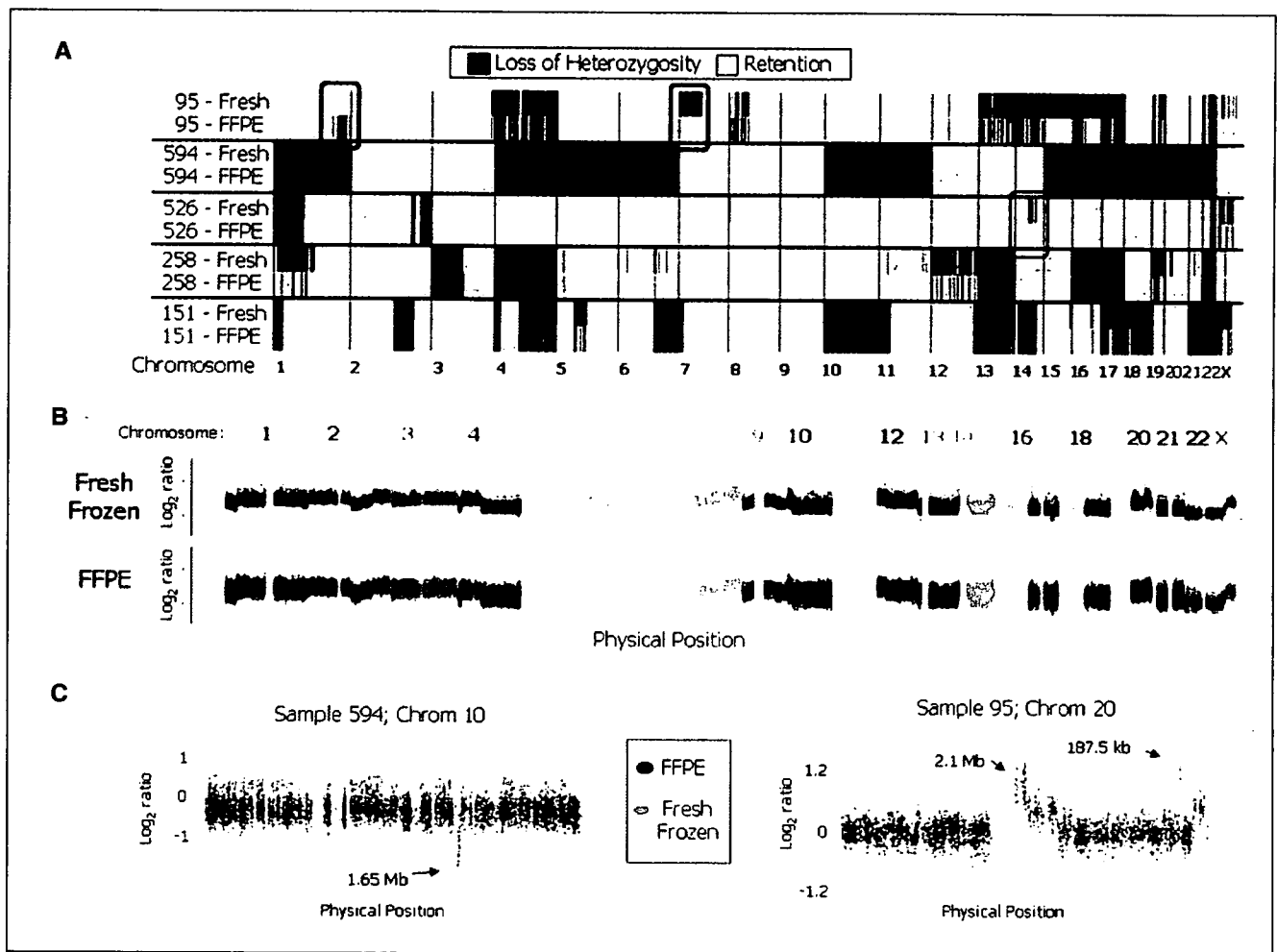


Figure 2. Genome-wide plots of LOH and copy number for fresh frozen and FFPE samples. **A**, genome-wide display of inferred LOH for fresh frozen and FFPE samples, including SNPs on fragments sizes ≤700 bp. *Blue regions*, LOH; *yellow regions*, retention of heterozygosity. Chromosome numbers are indicated below. Three discordant LOH predictions specific to either fresh frozen or FFPE samples were confirmed by microsatellite analysis of DNA (*brown boxes*, regions). **B**, raw single SNP log₂ ratios indicate gains and losses for fresh frozen (above) and FFPE (below) sources of sample 151 across the genome. Ratios represent copy number of tumor DNA over copy number of nontumor, non-FFPE lymphocytic DNA. Each color represents a different chromosome. SNPs were filtered for fragments ≤700 bp for the FFPE sample. **C**, raw single SNP log₂ ratios for fresh frozen (*orange*) and FFPE (*blue*) DNA are plotted across single chromosomes of multiple samples. SNPs were filtered for fragments ≤700 bp for FFPE data only. Highlighted copy number changes were confirmed by quantitative PCR.

Table 2. SNP numbers per fragment size filters

Fragment sizes included (bp)	250K Nsp array	250K Sty array	500K array set
≤300	13,636	15,845	29,481
≤400	39,492	45,473	84,965
≤500	74,372	82,099	156,471
≤600	113,687	120,025	233,712
≤650	133,748	138,282	272,030
≤700	153,198	155,590	308,788
≤800	190,899	187,687	378,586
≤850	209,017	201,004	410,021
≤900	222,316	213,300	435,616
≤1,000	244,644	230,527	475,171
Total	262,256	238,300	500,568

determine the optimal fragment size filter for copy number analysis. These plots can be viewed in CNAG_v2.0, and various fragment size filters can be applied until the mean copy number for the SNPs retained in analysis are consistent across fragment size (Fig. 4C, left). An example of this entire workflow is shown in Fig. 4A to C and results are listed in Supplementary Table S1. As shown for a 733-kb hemizygous loss highlighted in this example, the fragment size filter suggested by this process was able to increase the signal to noise ratio by preferentially removing the noisy SNPs instead of the informative SNPs and at the same time was also able to retain higher resolution by not overfiltering (Fig. 4C, right).

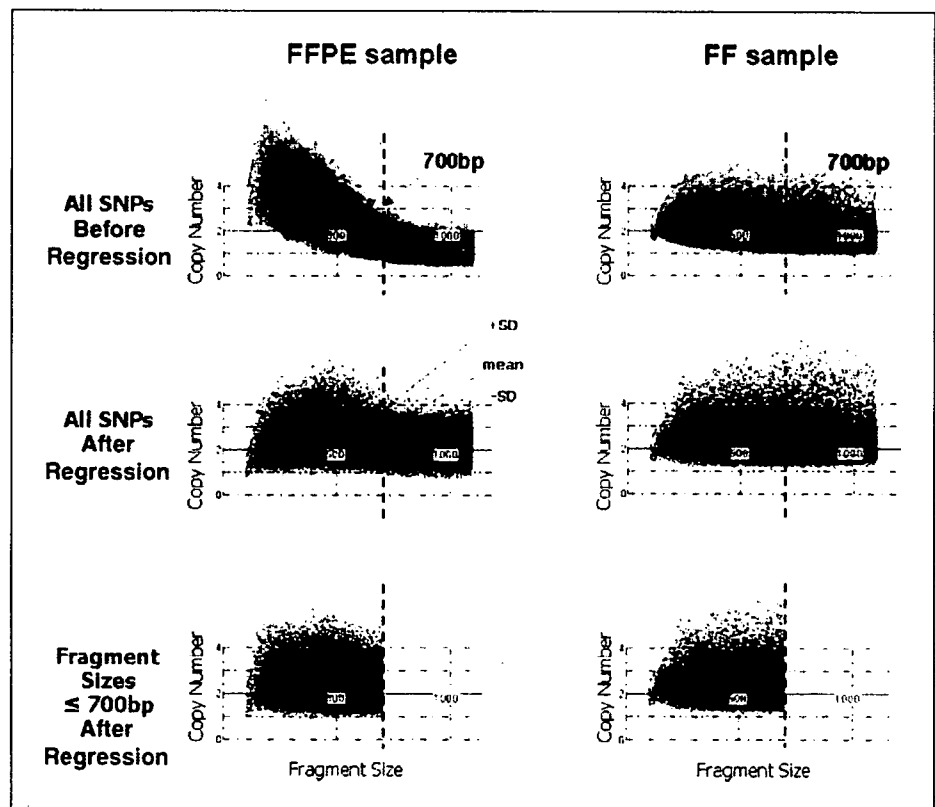
Years of storage and overall call rates displayed some correlation to copy number and call rate drop-off values, but PCR-based analyses had higher predictive power for these performance metrics (Fig. 4D). The Pearson's correlation of median RAPD-PCR values to copy number drop-off was 0.93, indicating high predictive power. Comparison of array performance to PCR-based DNA quality tests gave R^2 values above 0.8. In contrast, R^2 values were <0.7 when comparing performance with years of storage or comparing copy number drop-off with overall call rate. These results indicate that a PCR-based test of DNA quality is a reasonable method for predicting whether a FFPE DNA sample will be amenable to array analysis.

Six of the 25 samples (two breast and four colorectal) were not applied to the arrays because no RAPD-PCR products were produced. Sample 0588 also failed RAPD-PCR, but it was still applied to the array. Consistent with the RAPD-PCR prediction, this sample was the only example, in which call rates broken up by fragment size never exceeded 90%, and data from even the smallest fragment SNPs were too noisy for copy number analysis.

Discussion

There exists a large and growing deposit of archived clinical tissues, yet DNA extracted from these samples is usually degraded, contaminated, and of general low quality. This study expands the usefulness of the Mapping 500K arrays to DNA derived from FFPE samples, showing that the limiting factor for FFPE application is the size distribution of PCR amplicons during WGS. The maximum amplifiable fragment size, which is correlated to array performance, varied between samples and may be influenced by

Figure 3. Compensation against fragment size bias enables effective copy number analysis of FFPE samples. Raw predicted copy number (Y-axis) is influenced by fragment size (X-axis) in fresh frozen (right) and FFPE (left) samples, although the effect is exaggerated in the latter (see blue solid lines, middle). This causes an overestimate of copy number for fragments below ~500 bp and an underestimate for those above ~500 bp. Compensation against fragment size corrects this bias such that the mean predicted copy number (blue line) is constant independent of fragment size in fresh frozen samples (bottom right). For FFPE samples, exclusion of noninformative larger fragments before quadratic regression is required to effectively equilibrate copy number across maintained SNPs (top left).



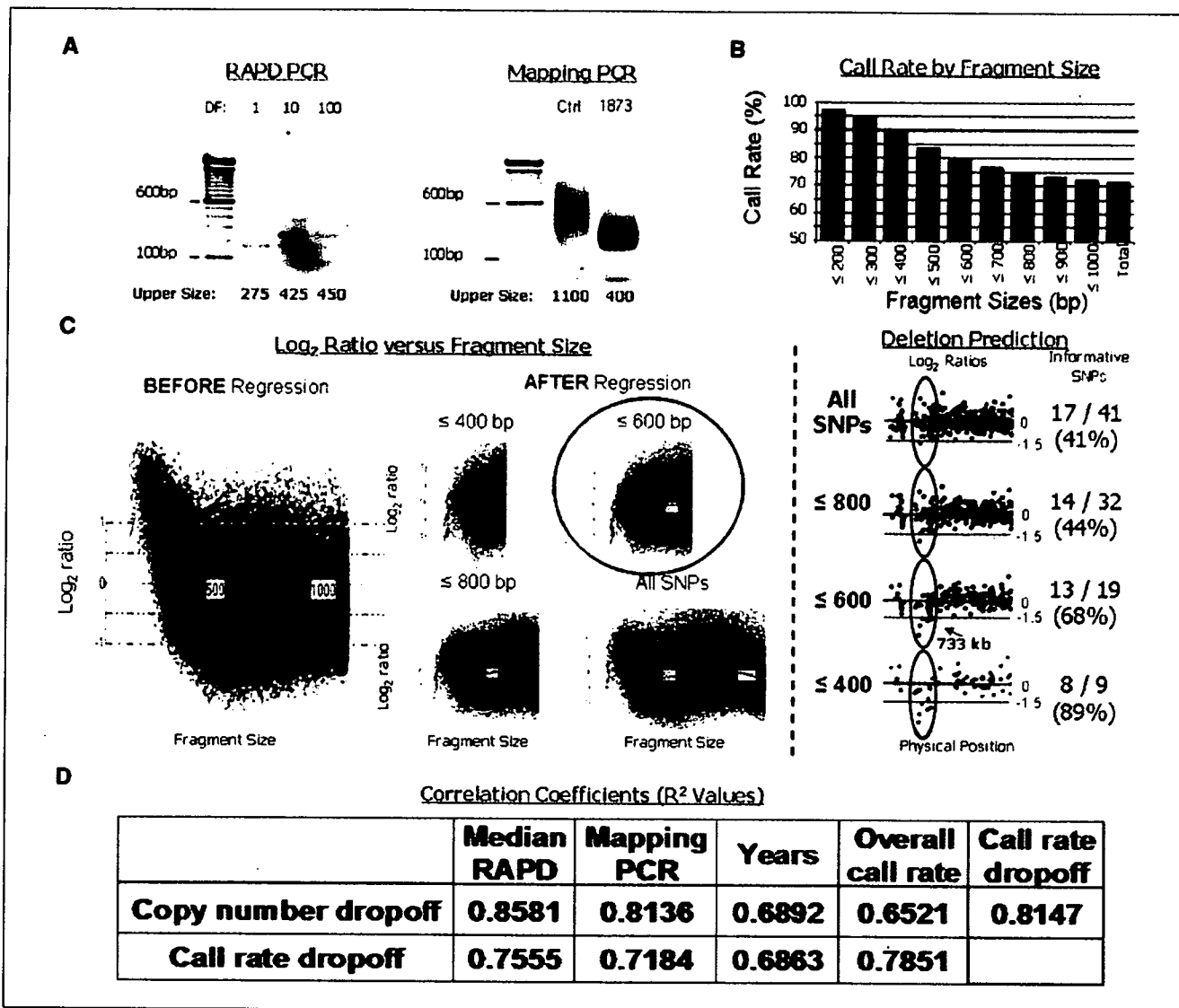


Figure 4. Prediction of FFPE sample performance. **A**, display of RAPD-PCR and Mapping assay PCR for a single breast tumor sample (1873). Maximum size amplicons from RAPD-PCR varied from 275 to 450 bp, with dilution factors (DF) of 1, 10, and 100. Although high-quality DNA had a maximum upper fragment size of ~1,100 after PCR during the Mapping assay, this sample was well amplified only up to ~400 bp. **B**, call rate by fragment size was monitored for the same sample, using a stringent confidence value threshold of 0.26. Call rates dropped <90% when excluding SNPs on fragment sizes >400 bp. **C**, copy number versus fragment size plots in CNAG_v2.0 show a strong influence by fragment size on copy number predictions before correction (*left*). Regression corrects this bias somewhat, and more and more stringent filters further correct this bias (*middle*). With a filter excluding SNPs on fragment sizes >600 bp, the mean copy number (*blue line*) is consistent regardless of fragment size, indicating that this sample requires a copy number filter at 600 bp. Log₂ ratios produced using various fragment size filters are displayed for a region containing a 733-kb deletion on part of chromosome X. Under "Informative SNPs," the number of SNPs predicting a deletion with a log₂ ratio below -0.3 (considered to be "informative") are listed to the left of the number of total SNPs within the deletion region that were retained during the fragment size filter. Below these values is the percentage of SNPs included in the analysis that were informative of the deletion. **D**, R² regression values when the fragment size at which call rates drop <90% or the maximum fragment size that can be included in copy number analyses are compared with median maximum RAPD-PCR amplicon size, maximum Mapping PCR amplicon size, years of storage, or overall call rate ($P \leq 0.26$) are displayed. PCR tests better predicted copy number performance than years of storage or overall call rate, and they were better predictors of genotype performance than years of storage was.

both extent of DNA degradation and modification as well as the amount of inhibitors remaining in the sample. Use of a suitable DNA extraction protocol, such as the DNeasy Tissue kit, is important for obtaining DNA amenable to the assay, but other factors, such as years of storage and fixation process, will be harder to control. This underscores the necessity for a pre-WGSA quality control step that includes PCR of larger fragment sizes, such as RAPD-PCR or multiplex PCR (16). This study attempts to outline guidelines for qualifying FFPE DNA samples and analyzing qualified

samples, but not all FFPE blocks will yield DNA suitable for the Mapping arrays.

FFPE DNA that is applied to the arrays may still vary in quality and therefore require more or less stringent fragment size filters. Despite reduction in coverage to accommodate loss of larger fragments, high resolution for genotype, LOH, and copy number assessment can still be maintained (Table 2; Supplementary Fig. S1). This is true because of the large number of SNPs on small fragments and because fragment size seems to be the only limiting

factor. For example, with exclusion of SNPs on amplicons >700 bp, as was required for the first set of five FFPE samples, 308,788 SNPs were retained for analysis, providing a median and mean inter-SNP distance of 4.3 or 9.5 kb, respectively. Although the 10K array is also suitable for analysis of degraded DNA (3), the large SNP coverage and the small fragment emphasis of the Mapping 500K arrays make it ideal for FFPE sample analysis.

The percentage of FFPE samples archived in banks that could be applied to the arrays with limited loss in genomic resolution would be influenced by the methods of fixation and extraction used at various institutes. Importantly, all samples stored for 6 years or fewer provided copy number data for a minimum of 234K SNPs in this study. Some of the samples applied to the arrays required extremely stringent filters against fragment size, resulting in significantly decreased resolution of genomic data. Potentially, researchers may choose only to analyze DNA samples of such low quality when the FFPE sample is considered to be particularly precious. Importantly, RAPD-PCR results predicted that these samples would display decreased performance on the array and a PCR screen could be applied to avoid application of poorly doing samples. With the advent of more standardized protocols for sample processing in the future and with advances in DNA extraction, a higher proportion of FFPE samples may be applicable to the arrays.

Despite the large banks of FFPE samples available for retrospective studies that include follow-up analysis of patient outcome, most of these studies currently focus on frozen samples because of the limited options available for paraffin samples. Additionally, FFPE processing holds advantages for tissue storage during prospective studies, in which many biopsies are collected but only a fraction of them are applied to downstream assays with selection based on clinical outcome. These results outline guidelines for the application of FFPE samples to the same genome-wide platform already available to high-quality DNA samples, thus enabling widespread retrospective and prospective analysis of tumor samples in their most common form of storage.

Acknowledgments

Received 10/2/2006; revised 12/19/2006; accepted 1/8/2007.

Grant support: National Breast Cancer Foundation postgraduate research scholarship (E.R. Thompson).

The costs of publication of this article were defrayed in part by the payment of page charges. This article must therefore be hereby marked *advertisement* in accordance with 18 U.S.C. Section 1734 solely to indicate this fact.

We would like to thank Giulia Kennedy, Manqin Cao, Yaron Turjuz, and Guoliang Xing for technical input and discussions, Michael Shaperro for his helpful suggestions and critical reading of the manuscript, and Dr. Alex Dobrovic for his help with DNA extraction.

References

- Wang Y, Moorhead M, Karlin-Neumann G, et al. Allele quantification using molecular inversion probes (MIP). *Nucleic Acids Res* 2005;33:e183.
- Lips EH, Dierssen JW, van Eijk R, et al. Reliable high-throughput genotyping and loss-of-heterozygosity detection in formalin-fixed, paraffin-embedded tumors using single nucleotide polymorphism arrays. *Cancer Res* 2005;65:10188-91.
- Thompson ER, Herbert SC, Forrest SM, Campbell IG. Whole genome SNP arrays using DNA derived from formalin-fixed, paraffin-embedded ovarian tumor tissue. *Hum Mutat* 2005;26:384-9.
- Kennedy GC, Matsuzaki H, Dong S, et al. Large-scale genotyping of complex DNA. *Nat Biotechnol* 2003;21:1233-7.
- Bryan EJ, Watson RH, Davis M, Hitchcock A, Foulkes WD, Campbell IG. Localization of an ovarian cancer tumor suppressor gene to a 0.5-cM region between D22S284 and CYP2D, on chromosome 22q. *Cancer Res* 1996;56:719-21.
- Jiang X, Hitchcock A, Bryan EJ, et al. Microsatellite analysis of endometriosis reveals loss of heterozygosity at candidate ovarian tumor suppressor gene loci. *Cancer Res* 1996;56:3534-9.
- Mullenbach R, Lagoda PJ, Welter C. An efficient salt chloroform extraction of DNA from blood and tissues. *Trends Genet* 1989;5:391.
- Bancroft JD, Stevens A. *Theory and practice of histological techniques*. 3rd ed. London: Churchill Livingstone; 1991. p. 48-57.
- Wu L, Patten N, Yamashiro CT, Chui B. Extraction and amplification of DNA from formalin-fixed, paraffin-embedded tissues. *Appl Immunohistochem Mol Morphol* 2002;10:269-74.
- Williams JG, Kubelik AR, Livak KJ, Rafalski JA, Tingey SV. DNA polymorphisms amplified by arbitrary primers are useful as genetic markers. *Nucleic Acids Res* 1990;18:6531-5.
- Siwoski A, Ishkanian A, Garnis C, Zhang L, Rosin M, Lam WL. An efficient method for the assessment of DNA quality of archival microdissected specimens. *Mod Pathol* 2002;15:889-92.
- Di X, Matsuzaki H, Webster TA, et al. Dynamic model based algorithms for screening and genotyping over 100 K SNPs on oligonucleotide microarrays. *Bioinformatics* 2005;21:1958-63.
- Lin M, Wei LJ, Sellers WR, Lieberfarb M, Wong WH, Li C. dChipSNP: significance curve and clustering of SNP-array-based loss-of-heterozygosity data. *Bioinformatics* 2004;20:1233-40.
- Huang J, Wei W, Zhang J, et al. Whole genome DNA copy number changes identified by high density oligonucleotide arrays. *Hum Genomics* 2004;1:287-99.
- Nannya Y, Sanada M, Nakazaki K, et al. A robust algorithm for copy number detection using high-density oligonucleotide single nucleotide polymorphism genotyping arrays. *Cancer Res* 2005;65:6071-9.
- van Beers EH, Joosse SA, Ligtenberg MJ, et al. A multiplex PCR predictor for aCGH success of FFPE samples. *Br J Cancer* 2006;94:333-7.
- Liu WM, Di X, Yang G, et al. Algorithms for large-scale genotyping microarrays. *Bioinformatics* 2003;19:2397-403.



Functional characterization of a new p53 mutant generated by homozygous deletion in a neuroblastoma cell line

Yohko Nakamura¹, Toshinori Ozaki¹, Hidetaka Niizuma, Miki Ohira, Takehiko Kamijo, Akira Nakagawara*

Division of Biochemistry, Chiba Cancer Center Research Institute, Chiba 260-8717, Japan

Received 11 January 2007

Available online 22 January 2007

Abstract

p53 is a key modulator of a variety of cellular stresses. In human neuroblastomas, p53 is rarely mutated and aberrantly expressed in cytoplasm. In this study, we have identified a novel p53 mutant lacking its COOH-terminal region in neuroblastoma SK-N-AS cells. p53 accumulated in response to cisplatin (CDDP) and thereby promoting apoptosis in neuroblastoma SH-SY5Y cells bearing wild-type p53, whereas SK-N-AS cells did not undergo apoptosis. We found another p53 (p53ΔC) lacking a part of oligomerization domain and nuclear localization signals in SK-N-AS cells. p53ΔC was expressed largely in cytoplasm and lost the transactivation function. Furthermore, a 3'-part of the p53 locus was homozygously deleted in SK-N-AS cells. Thus, our present findings suggest that p53 plays an important role in the DNA-damage response in certain neuroblastoma cells and it seems to be important to search for p53 mutations outside DNA-binding domain.

© 2007 Elsevier Inc. All rights reserved.

Keywords: Apoptosis; Cisplatin; Homozygous deletion; Neuroblastoma; p53

p53 plays a pivotal role in the regulation of cell cycle arrest and apoptosis. p53 is one of the most frequently mutated genes in human tumors [1,2] and p53-deficient mice developed spontaneous tumors [3]. Upon a variety of cellular stresses, p53 accumulates in nucleus through post-translational modifications including phosphorylation and acetylation and thereby exerting its function [4]. Pro-apoptotic function of p53 is closely linked to its DNA-binding activity. p53 acts as a transcription factor to transactivate a variety of its target genes. Indeed, 95% of p53 mutations in human tumors occur within its DNA-binding region and these mutations inactivate pro-apoptotic function of p53 [4].

Alternatively, p53 is inhibited by various mechanisms. MDM2 acts as an E3 ubiquitin ligase for p53 and promotes

its proteolytic degradation through ubiquitin-proteasome pathway [5,6]. Subcellular distribution of p53 also plays a key role in the regulation of p53 [4]. p53 contains three nuclear localization signals (NLS I, II, and III) in its COOH-terminal region [7,8]. In contrast to other human tumors, p53 is rarely mutated in neuroblastomas [9]. Neuroblastoma cells showed a cytoplasmic localization of wild-type p53 and exhibited an impaired p53-mediated cell cycle arrest in response to DNA damage, suggesting that there exists a mutation-independent mechanism of p53 inactivation [10–12]. Intriguingly, Nikolaev et al. demonstrated that Parkin-like ubiquitin ligase termed Parc serves as an anchor protein that tethers p53 in cytoplasm and thereby regulating subcellular localization and function of p53 [13].

In this study, we have identified a novel p53 mutant (p53ΔC) homozygously deleted in neuroblastoma SK-N-AS cells and our current studies suggest that p53 status plays an important role in the cell fate determination of certain neuroblastoma cells in response to DNA damage.

* Corresponding author. Fax: +81 43 265 4459.

E-mail address: akiranak@chiba-cc.jp (A. Nakagawara).

¹ These authors contributed equally to this work.

Materials and methods

Cell culture and transfection. Neuroblastoma cells were grown in RPMI 1640 medium supplemented with 10% heat-inactivated fetal bovine serum (FBS, Invitrogen) and antibiotic mixture in a humidified atmosphere of 5% CO₂ in air at 37 °C. For transfection, cells were transfected with the indicated expression plasmids using LipofectAMINE 2000 according to the manufacturer's instructions (Invitrogen).

Construction of p53 mutant. cDNA encoding p53 mutant was amplified by PCR using cDNA from SK-N-AS cells. Forward and reverse primers were 5'-AATATTTACCCCTTCAGGTACTAAG-3' (forward) and 5'-CTCGAGTCACTGCCCTTGATGGC-3' (reverse). *SspI* and *XhoI* sites shown in boldface type were introduced into forward and reverse primers, respectively. PCR products were gel-purified and subcloned into pGEM-T plasmid (Promega). Constructs were confirmed by sequencing and then digested with *SspI* and *XhoI*. The digested fragment was again gel-purified and then ligated with the *SspI* and *BamHI* fragment of FLAG-p53 to give pcDNA3-FLAG-p53CA.

RNA preparation and RT-PCR analysis. Total RNA was prepared using RNeasy Mini kit (Qiagen) following the manufacturer's protocol. cDNA was synthesized using SuperScript II with random primers (Invitrogen) and amplified by PCR using primers as described: *p53*: forward, 5'-CTGCCCTCAACAAGATGTTTGTG-3', and reverse, 5'-CTA TCTGAGCAGCGCTCATGG-3'; *p21^{WAF1}*: forward, 5'-ATGAAAATTCACCCCTTTCC-3', and reverse, 5'-CCCTAGGCTGTGCTCACTTC-3'; *Bax*: forward, 5'-TTTGCTTCAGGGTTTCATCC-3', and reverse, 5'-CAGTTGAAGTTGCCGTCAGA-3'; *p53AIP1*: forward, 5'-CCAAGTCTCTGCTTTC-3' and reverse, 5'-AGCTGAGCTCAAATGCTGAC-3'; *PUMA*: forward, 5'-TATGGATCCCGCACCATGGACTACAAGGACGACGATGACAAGGCCCGCGCACGCCAG-3' and reverse, 5'-TATGGATCCCTACATGGTGCAGAGAAAGTCCCCC-3'; and *GAPDH*: forward, 5'-ACCTGACCTGCCGTCTAGAA-3', and reverse, 5'-TCCA CACCCTGTGTCTGA-3'.

Southern blotting. Genomic DNA was digested with *PvuI*, separated by 1% agarose gel electrophoresis, and transferred onto nylon membranes. Hybridization was performed at 65 °C in a solution containing 1 M NaCl, 1% *N*-lauroyl sarcosine, 7.5% dextran sulfate, 100 µg of heat-denatured salmon sperm DNA/ml, and radio-labeled DNA. After hybridization, membranes were washed twice with 2× SSC/0.1% *N*-lauroyl sarcosine at 50 °C and exposed to an X-ray film at -70 °C.

Immunoblotting. Cells were lysed in lysis buffer containing 25 mM Tris-HCl, pH 8.0, 137 mM NaCl, 2.7 mM KCl, 1% Triton X-100, and protease inhibitor mixture (Sigma). Lysates were separated by SDS-PAGE and transferred onto Immobilon-P membranes (Millipore). Membranes were probed with anti-p53 (DO-1, Calbiochem), anti-p53 (PAb122, BD Pharmingen), anti-phosphorylated p53 at Ser-15 (Cell Signaling) or with anti-actin (20 33, Sigma) followed by incubation with HRP-conjugated goat anti-mouse or anti-rabbit IgG secondary antibody (Cell Signaling). Immunoreactive bands were detected using chemiluminescence (ECL, Amersham Biosciences).

Subcellular fractionation. Cells were lysed in lysis buffer containing 10 mM Tris HCl, pH 7.5, 1 mM EDTA, 0.5% NP-40, and protease inhibitor mixture (Sigma). Lysates were centrifuged to separate soluble (cytosolic) from insoluble (nuclear) fractions. The nuclear and cytosolic fractions were subjected to immunoblotting using anti-p53, anti-Lamin B (Ab-1, Oncogene Research products) or with anti-tubulin- α (Ab-2, NeoMarkers).

Array-based comparative genomic hybridization (CGH) analysis. Whole genome arrays of 2464 bacterial artificial chromosome (BAC) clones were hybridized simultaneously with 500 ng of target DNA (SK-N-AS, RTBM1, and SH-SY5Y) and reference DNA (normal female genomic DNA). Target DNAs were labeled with Cy3-dCTP and reference DNAs with Cy5-dCTP by random priming. Hybridization, scanning, and data processing were conducted as described previously [14,15].

Cell survival assays. Cells were plated at a density of 5000 cells/well in 96-well tissue culture plates. After attachment overnight, medium was replaced and treated with CDDP for 24 h. Cell viability was measured by MTT assay.

Flow cytometry. Floating and adherent cells were pooled and fixed in ice-cold 70% ethanol for 4 h at -20 °C. Cells were then stained with 10 mg/ml of PI (Sigma) in the presence of 250 mg/ml of RNase A at 37 °C for 30 min in the dark. Number of cells with sub-G1 DNA content was measured by flow cytometry (FACScan, Becton Dickinson).

TUNEL assay. Apoptotic cells were identified using an *in situ* cell detection, peroxidase kit (Roche Applied Science). Briefly, cells were fixed in 4% paraformaldehyde and permeabilized with 0.1% Triton X-100. The labeling reaction was performed using TMR red-labeled dUTP together with other nucleotides by terminal deoxynucleotidyl transferase for 1 h in the dark at 37 °C. Then, cells were mounted and the incorporated TMR red-labeled dUTP was analyzed using a Fluoview laser scanning confocal microscope (Olympus).

Luciferase reporter assay. H1299 cells were co-transfected with pcDNA3, FLAG-p53 or FLAG-p53AC expression plasmid, p53-responsive luciferase reporter (*p21^{WAF1}*, *MDM2* or *Bax*), and pRL-TK *Renilla* luciferase cDNA. Forty-eight hours after transfection, firefly and *Renilla* luciferase activities were measured with dual-luciferase reporter assay system according to the manufacturer's instructions (Promega).

Colony formation assay. Forty-eight hours after transfection, SK-N-AS cells were transferred to fresh medium containing G418 (400 µg/ml). After 16 days of selection, drug-resistant colonies were fixed in methanol and stained with Giemsa's solution.

Results

DNA-damage response in human neuroblastoma cells

To determine the effects of genotoxic agents on neuroblastomas, human neuroblastoma SH-SY5Y and SK-N-AS cells were exposed to cisplatin (CDDP) and their viabilities were examined by MTT assays. As shown in Fig. 1A, their viabilities were significantly decreased in response to CDDP. To address whether CDDP could induce apoptosis, we performed TUNEL assay. As shown in Fig. 1B, we observed a higher number of TUNEL-positive SH-SY5Y cells exposed to CDDP, whereas CDDP had undetectable effects on SK-N-AS cells. We further determined apoptotic cells as sub-G1 population by flow cytometry. As seen in Fig. 1C, a significant increase in number of SH-SY5Y cells with sub-G1 DNA content was observed after CDDP treatment, whereas CDDP treatment of SK-N-AS cells resulted in an increase in S-phase cells but not in G2/M-phase cells. Consistent with these results, *thymidine kinase* (S-phase marker) [16] was increased in CDDP-treated SK-N-AS cells, whereas *Plk1* (M-phase marker) [17] remained unchanged regardless of CDDP treatment (data not shown).

We then examined whether p53-dependent apoptotic pathway could be activated in response to CDDP. As shown in Fig. 1D, p53 was phosphorylated at Ser-15 in SH-SY5Y cells exposed to CDDP. p53 remained unchanged regardless of CDDP treatment, whereas p53 target genes including *p21^{WAF1}*, *Bax*, and *PUMA* were transactivated in response to CDDP. In contrast, CDDP-mediated phosphorylation of p53 at Ser-15 was undetectable in SK-N-AS cells. *p21^{WAF1}* was induced in response to CDDP, however, CDDP-mediated up-regulation of pro-apoptotic *Bax* and *PUMA* was undetectable, suggesting that p53 pro-apoptotic function might be lost in SK-N-AS cells.

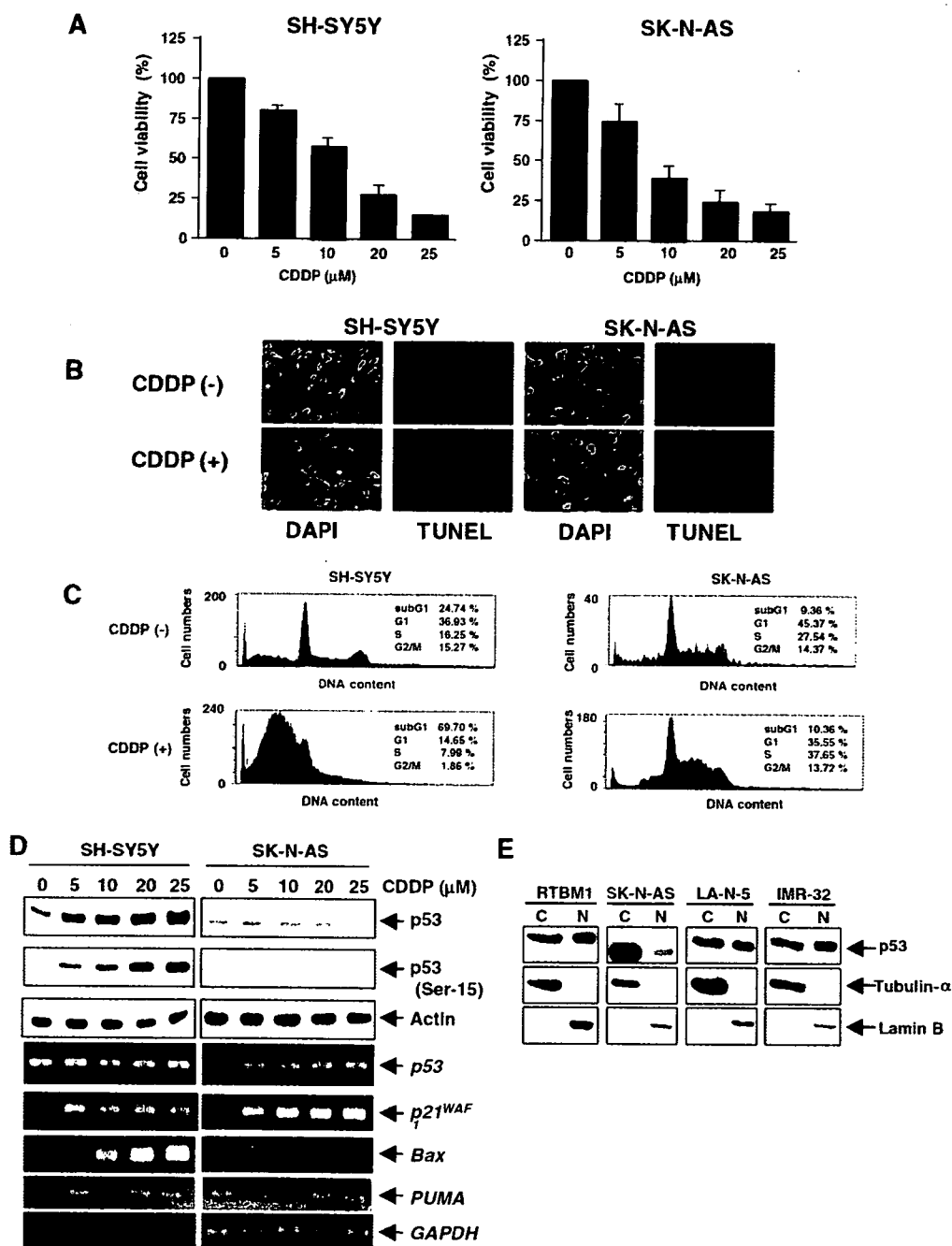


Fig. 1. Differential effects of CDDP on neuroblastoma cells. (A) Cell survival assays. Twenty-four hours after CDDP treatment, cell viability was analyzed by MTT assays. (B) TUNEL staining. Twenty-four hours after CDDP treatment (20 μ M), apoptotic cells were detected by TUNEL staining. Cell nuclei were stained with DAPI. (C) FACS analysis. SH-SY5Y and SK-N-AS cells were treated as in (B). Twenty-four hours after CDDP treatment, cell cycle distributions were analyzed by FACS. Shown are the representatives of three independent experiments. (D) CDDP-induced accumulation of p53 in neuroblastoma cells. Twenty-four hours after CDDP treatment, lysates and total RNA were subjected to immunoblotting (upper panels) and RT-PCR (lower panels), respectively. For protein loading control, actin levels were checked by immunoblotting. For RT-PCR, *GAPDH* was used as a loading control. (E) Subcellular localization of p53. The indicated neuroblastoma cells were fractionated into cytoplasmic (C) and nuclear (N) fractions and subcellular distribution of p53 was analyzed by immunoblotting. Tubulin- α and Lamin B were used as cytoplasmic and nuclear markers, respectively.

To investigate molecular mechanism(s) behind p53 dysfunction in SK-N-AS cells, we examined subcellular localization of p53 in various neuroblastoma cells. As shown in Fig. 1E, p53 was detected in cytoplasm and

nucleus of RTBM1, LA-N-5, and IMR-32 cells bearing wild-type *p53* (data not shown). Of note, p53 was abundantly expressed in cytoplasm of SK-N-AS cells and its molecular mass was smaller than those of other

cells, indicating that it might be due to certain structural aberrations.

Structural aberration of p53 in SK-N-AS cells

To address whether p53 could have any aberrations in SK-N-AS cells; we amplified the indicated genomic regions of p53 using genomic DNA from SK-N-AS cells. RTBM1 cells were used as a positive control. As shown in Fig. 2A, PCR-based amplification using primer sets including P1, P2, P6, and P7 successfully generated estimated sizes of PCR products, whereas remaining primer sets (P3–P5) did not, suggesting that the genomic region containing exons 10 and 11 of p53 might be lost in SK-N-AS cells.

To confirm genomic aberrations within p53 locus in SK-N-AS cells, we performed Southern analysis. Radio-labeled p53 cDNA probe failed to detect PstI fragment (2.0 kb in length) which contains exons 10 and 11 in SK-N-AS cells (Fig. 2B). Our array-based comparative genomic hybridization (CGH) analysis demonstrated that there exists a large range of allelic deletion of chromosome 17p where p53 is located in SK-N-AS cells (Fig. 2C). Furthermore,

anti-p53 antibody which recognizes p53 extreme COOH-terminal portion could not detect p53 in SK-N-AS cells (Fig. 2D). Collectively, our results suggest that p53 COOH-terminal region is homozygously deleted in SK-N-AS cells. We then cloned p53 cDNA. As shown in Fig. 2E, a newly identified p53 (p53ΔC) was composed of 369 amino acids including unique COOH-terminal structure (estimated molecular mass of 49 kDa), lacked a part of oligomerization domain, and completely lost NLS II and III. The 3'-side of intron 9 and the downstream region containing exons 10 and 11 were deleted in SK-N-AS cells. Its unique COOH-terminal amino acids were derived from intron 9, suggesting that accurate splicing event might be abrogated and thereby generating p53ΔC.

Dysfunction of p53ΔC

To ask whether p53ΔC could have functional differences as compared with wild-type p53, FLAG-p53 or FLAG-p53ΔC was expressed in SK-N-AS cells and their subcellular localization was examined. As shown in Fig. 3A, FLAG-p53 was detectable in cytoplasm and nucleus,

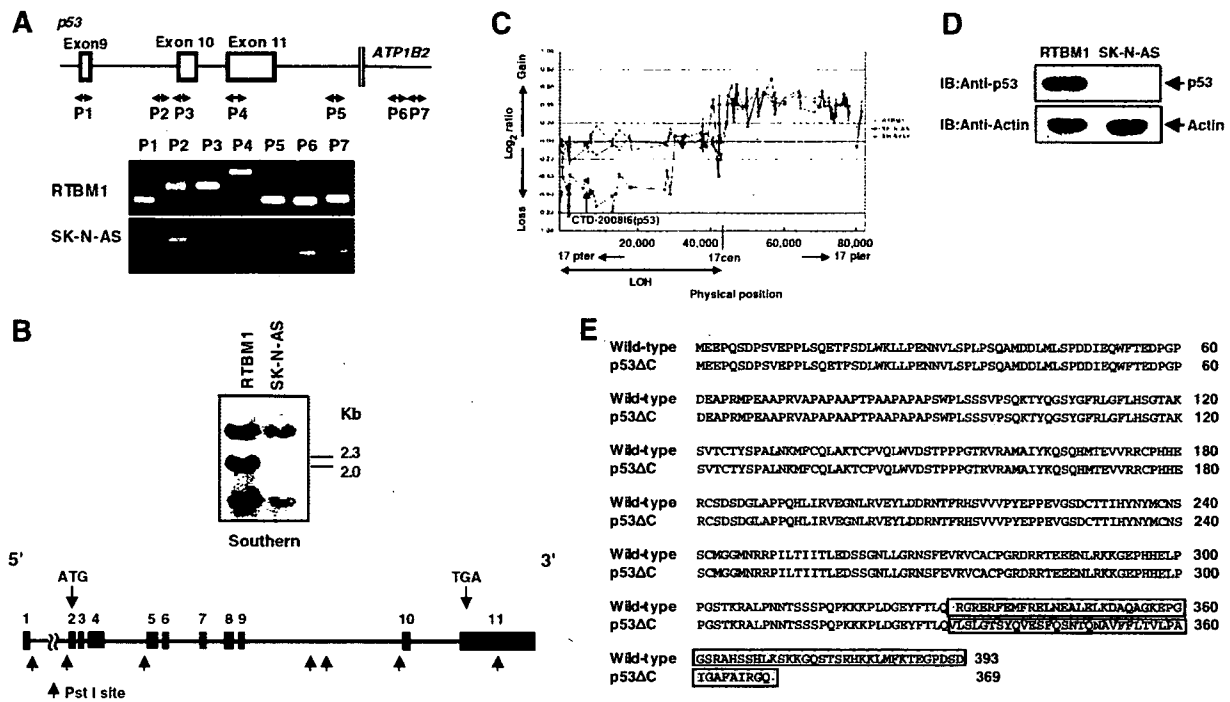


Fig. 2. p53 COOH-terminal region is deleted in SK-N-AS cells. (A) Genomic structure of human p53 locus and positions of PCR primers (P1–P7) are shown. ATP1B2 encodes ATPase. Na⁺/K⁺ transporting β2 (upper panel). Genomic DNA from RTBM1 and SK-N-AS cells was subjected to PCR using the indicated primers (lower panels). (B) Southern blot analysis. Genomic DNA was digested with PstI, separated by 1% agarose gel, transferred onto nylon membrane, and probed with the radio-labeled p53 cDNA. Schematic diagram of human p53 and positions of PstI sites are also shown. (C) Array-based comparative genomic hybridization (CGH) analysis. Hybridization was performed as described under Materials and methods. Arrays were scanned and images processed using custom software. We normalized relative ratios of tumor and normal signals by setting the value of the median relative ratio equal to 1. The data were then transformed into log₂ space and plotted as a histogram for scoring loss or gain. Three Gaussian distribution curves were fitted to the histogram, and values ± 3 SD from the central Gaussian were scored as losses or gains for that tumor. (D) Immunoblotting. Lysates from RTBM1 and SK-N-AS were processed for immunoblotting with the specific antibody against p53 extreme COOH-terminal portion. (E) Amino acid sequence alignment of wild-type p53 and p53ΔC. The different amino acid residues between them are boxed.

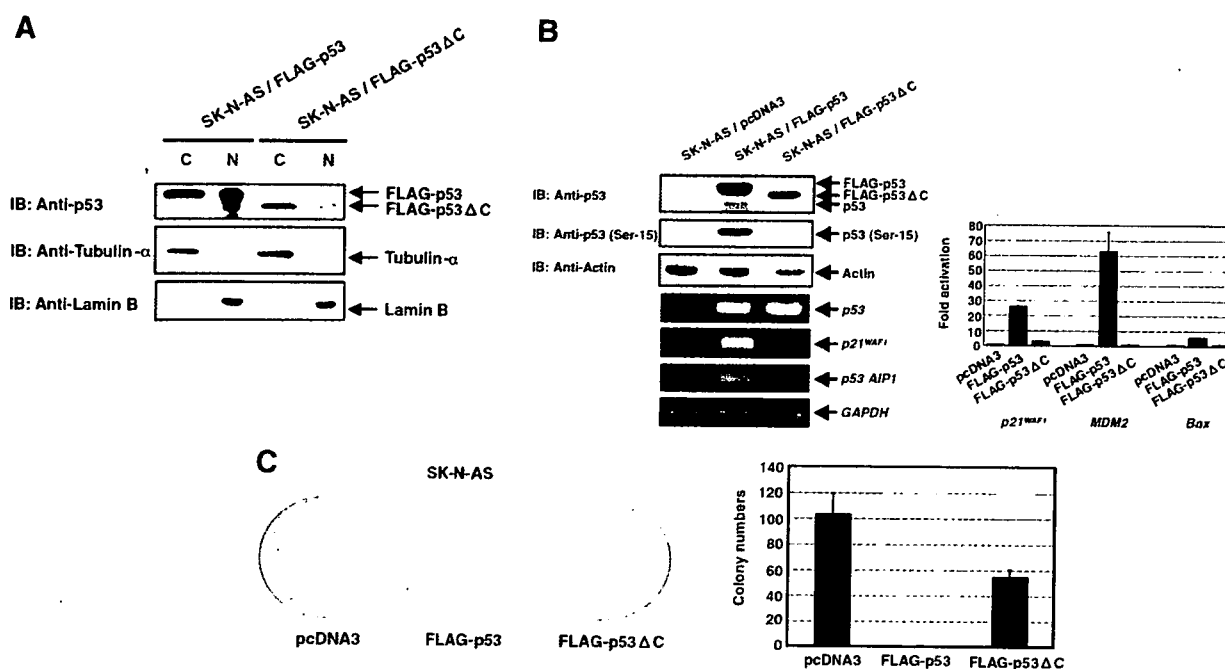


Fig. 3. Loss of function of p53 Δ C. (A) Subcellular localization of exogenously expressed wild-type p53 and p53 Δ C. SK-N-AS cells were transfected with the indicated expression plasmids. Forty-eight hours after transfection, cells were fractionated into cytoplasmic (C) and nuclear (N) fractions followed by immunoblotting with anti-p53 antibody. (B) Possible effects of COOH-terminal deletion of p53 on its transcriptional activity. SK-N-AS cells were transfected with the indicated expression plasmids. Forty-eight hours after transfection, lysates and total RNA were subjected to immunoblotting and RT-PCR, respectively (left panel). (Right panel) Luciferase reporter assays. p53-deficient H1299 cells were co-transfected with pcDNA3, FLAG-p53 or FLAG-p53 Δ C expression plasmid, p53-responsive luciferase reporter (*p21^{WAF1}*, *MDM2* or *Bax*) and *Renilla* luciferase cDNA. Forty-eight hours after transfection, luciferase activities were measured. (C) Colony formation assay. SK-N-AS cells were transfected to fresh medium containing G418 (400 μ g/ml). Sixteen days after selection with G418, drug-resistant colonies were stained with Giemsa's solution (left panel) and the number of colonies was scored (right panel).

whereas FLAG-p53 Δ C was largely expressed in cytoplasm. Next, we examined transcriptional potential of p53 Δ C in SK-N-AS cells. As seen in left panel of Fig. 3B, FLAG-p53 but not FLAG-p53 Δ C was phosphorylated at Ser-15. Consistent with these results, FLAG-p53 transactivated *p21^{WAF1}* and *p53AIP1*. In contrast, FLAG-p53 Δ C failed to transactivate *p21^{WAF1}* and *p53AIP1*. Similar results were also obtained by luciferase reporter assays (Fig. 3B, right panel). To examine effects of COOH-terminal deletion on pro-apoptotic activity of p53, we performed colony formation assays. SK-N-AS cells were transfected with empty plasmid, FLAG-p53 or FLAG-p53 Δ C expression plasmid and maintained in medium containing G418 for 16 days. As shown in Fig. 3C, number of drug-resistant colonies was significantly reduced in cells expressing FLAG-p53. Intriguingly, enforced expression of FLAG-p53 Δ C resulted in a decrease in number of drug-resistant colonies but to a lesser degree as compared with that in cells expressing FLAG-p53. These observations suggest that COOH-terminal deletion reduces transcriptional and pro-apoptotic activities of p53.

Discussion

In this study, we have identified p53 Δ C in SK-N-AS cells. Consistent with the recent report [13], p53 was

predominantly expressed in cytoplasm of SK-N-AS cells. According to their results, Parc inhibited p53 nuclear translocation through the direct interaction with its COOH-terminal region. Since p53 contains three NLSs in its COOH-terminal region, Parc might inhibit its nuclear access by masking its NLSs [13]. In accordance with these findings, p53 COOH-terminal peptide inhibited its cytoplasmic retention [12]. Based on our immunoprecipitation experiments, wild-type p53 but not p53 Δ C was co-immunoprecipitated with the endogenous Parc in SK-N-AS cells (data not shown), suggesting that cytoplasmic retention of p53 Δ C is regulated in a Parc-independent manner. p53 Δ C lacks NLS II and III but retains NLS I. Although Kim et al. described that importin- α interacts with NLS I of p53 and mediates its nuclear import [18], NLS II and/or III might play a major role in nuclear import of p53 in SK-N-AS cells.

p53 phosphorylation is significantly associated with its pro-apoptotic function [4]. Exogenously expressed wild-type p53 but not p53 Δ C was phosphorylated at Ser-15 in SK-N-AS cells without DNA damage and transactivated *p21^{WAF1}* and *p53AIP1*. Rodicker and Putzer described that exogenously expressed p53 is phosphorylated at Ser-15 without DNA damage [19]. Although it is unknown why exogenously expressed p53 but not p53 Δ C is phosphorylated at Ser15 without DNA damage, it might be at least

in part due to its cytoplasmic retention. Colony formation assays demonstrated that wild-type p53 markedly reduces number of drug-resistant colonies in SK-N-AS cells, suggesting that there might not exist functional disruptions of downstream mediators of p53 in SK-N-AS cells. In response to CDDP, SH-SY5Y cells underwent apoptosis in association with a significant induction of p53. On the other hand, SK-N-AS cells did not undergo apoptosis in response to CDDP, suggesting that p53 status might determine neuroblastoma cell fate to survive or to die. Intriguingly, CDDP treatment of SK-N-AS cells induced an accumulation of S-phase cells accompanied with up-regulation of $p21^{WAF1}$. Since p53 ΔC failed to transactivate $p21^{WAF1}$ and CDDP had undetectable effects on $p73$ and $p63$ (other members of p53 family) (data not shown), CDDP-mediated up-regulation of $p21^{WAF1}$ in SK-N-AS cells is regulated in a p53 family-independent manner. Knudsen et al. reported that CDDP-mediated DNA damage induces an intra-S-phase cell cycle arrest, which is correlated with a protection against apoptosis [20]. Thus, the genome maintenance system might delay the onset of mitosis, and thereby providing time to complete DNA repair and/or DNA replication before cell division in SK-N-AS cells. Further efforts should be necessary to address this issue.

Majority of p53 mutations is detected within its DNA-binding region [21]. SK-N-AS cells have been believed to express wild-type p53 [22]. Much of information regarding p53 mutations was derived from sequence analysis of exons 5–8 which encode its DNA-binding domain [4]. Indeed, there exist missense mutations in p53 oligomerization domain [23]. According to their results, Leu to Pro substitution at 344 inhibited the oligomerization of p53 and abolished its DNA-binding activity. Since p53 ΔC lacks a part of oligomerization domain including Leu-344, p53 ΔC might exist as a monomeric latent form. Recently, Bourdon et al. described that human p53 is expressed as multiple isoforms including p53 β and p53 γ [24]. Based on amino acid sequence comparison, p53 ΔC was distinct from p53 β and p53 γ (data not shown). During the preparation of our manuscript, Goldschneider et al. reported that SK-N-AS cells express p53 β [25]. This discrepancy might be attributed to co-expression of p53 β and p53 ΔC in SK-N-AS cells and/or due to the acquired heterogeneity of SK-N-AS cells during culture. Additionally, murine p53 expresses an alternative splicing isoform termed ASp53 with different COOH-terminus from that of wild-type p53 [26]. ASp53 displays an enhanced transcriptional activity as compared with wild-type p53, indicating that p53 ΔC is distinct from human counterpart of ASp53.

Acknowledgments

This work was supported in part by a Grant-in-Aid from the Ministry of Health, Labor and Welfare for Third Term Comprehensive Control Research for Cancer, a Grant-in-Aid for Scientific Research on Priority

Areas from the Ministry of Education, Culture, Sports, Science and Technology, Japan, a Grant-in-Aid for Scientific Research from Japan Society for the Promotion of Science, and a Grant from Uehara Memorial Foundation.

References

- [1] M. Hollstein, D. Sidransky, B. Vogelstein, H. Harris, p53 mutations in human cancers, *Science* 253 (1991) 49–53.
- [2] A.J. Levine, J. Momand, C.A. Finlay, The p53 tumour suppressor gene, *Nature* 351 (1991) 453–456.
- [3] L.A. Donehower, M. Harvey, B.L. Slagle, M.J. McArthur, C.A. Montgomery Jr., J.S. Butel, A. Bradley, Mice deficient for p53 are developmentally normal but susceptible to spontaneous tumours, *Nature* 356 (1992) 215–221.
- [4] K.H. Vousden, X. Lu, Live or let die: the cells response to p53, *Nat. Rev. Cancer* 2 (2002) 594–604.
- [5] Y. Haupt, R. Maya, A. Kazaz, M. Oren, Mdm2 promotes the rapid degradation of p53, *Nature* 387 (1997) 296–299.
- [6] M.H.G. Kabbat, S.N. Jones, K.H. Vousden, Regulation of p53 stability by Mdm2, *Nature* 387 (1997) 299–303.
- [7] G. Shaulsky, N. Goldfinger, A. Ben-Ze'ev, V. Rotter, Nuclear accumulation of p53 protein is mediated by several nuclear localization signals and plays a role in tumorigenesis, *Mol. Cell. Biol.* 10 (1990) 6565–6577.
- [8] S.H. Liang, D. Hong, M.F. Clarke, Cooperation of a single lysine mutation and a C-terminal domain in the cytoplasmic sequestration of the p53 protein, *J. Biol. Chem.* 273 (1998) 19817–19821.
- [9] K. Vogan, M. Bernstein, J.M. Leclerc, L. Brisson, J. Brossard, G.M. Brodeur, J. Pelletier, P. Gros, Absence of p53 gene mutations in primary neuroblastomas, *Cancer Res.* 53 (1993) 5269–5273.
- [10] U.M. Moll, M. LaQuaglia, J. Benard, G. Riou, Wild-type p53 protein undergoes cytoplasmic sequestration in undifferentiated neuroblastomas but not in differentiated tumors, *Proc. Natl. Acad. Sci. USA* 92 (1995) 4407–4411.
- [11] U.M. Moll, A.G. Ostermeyer, R. Haladay, B. Winkfield, M. Frazier, G. Zambetti, Cytoplasmic sequestration of wild-type p53 protein impairs the G1 checkpoint after DNA damage, *Mol. Cell. Biol.* 16 (1996) 1126–1137.
- [12] A.G. Ostermeyer, E. Runko, B. Winkfield, B. Ahn, U.M. Moll, Cytoplasmically sequestered wild-type p53 protein in neuroblastoma is relocated to the nucleus by a C-terminal peptide, *Proc. Natl. Acad. Sci. USA* 93 (1996) 15190–15194.
- [13] A.Y. Nikolaev, M. Li, N. Puskas, J. Qin, W. Gu, Parc: A cytoplasmic anchor for p53, *Cell* 112 (2003) 29–40.
- [14] A.M. Snijders, N. Nowak, R. Segraves, S. Blackwood, N. Brown, J. Conroy, G. Hamilton, A.K. Hindle, B. Huey, K. Kimura, S. Law, K. Myambo, J. Palmer, B. Yistra, J.P. Yue, J.W. Gray, A.N. Jain, D. Pinkel, D.G. Albertson, Assembly of microarrays for genome-wide measurement of DNA copy number, *Nat. Genet.* 29 (2001) 263–264.
- [15] J.M. Nigro, A. Misra, L. Zhang, I. Smimov, H. Colman, C. Griffin, N. Ozburn, M. Chen, E. Pan, D. Koul, W.K. Yung, B.G. Feuerstein, K.D. Aldape, Integrated array-comparative genomic hybridization and expression array profiles identify clinically relevant molecular subtypes of glioblastoma, *Cancer Res.* 65 (2005) 1678–1686.
- [16] D.L. Coppock, A.B. Pardee, Control of thymidine kinase mRNA during the cell cycle, *Mol. Cell. Biol.* 7 (1987) 2925–2932.
- [17] R. Hamanaka, M.R. Smith, P.M. O'Connor, S. Maloid, K. Mihalic, J.L. Spivak, D.L. Longo, D.K. Ferris, Polo-like kinase is a cell cycle-regulated kinase activated during mitosis, *J. Biol. Chem.* 270 (1995) 21086–21091.
- [18] I.S. Kim, D.H. Kim, S.M. Han, M.U. Chin, H.J. Nam, H.P. Cho, S.Y. Choi, B.J. Song, E.R. Kim, Y.S. Bae, Y.H. Moon, Truncated form of importin α identified in breast cancer cell inhibits nuclear import of p53, *J. Biol. Chem.* 275 (2000) 23139–23145.

- [19] F. Rodicker, B.M. Putzer, p73 is effective in p53-null pancreatic cancer cells resistant to wild-type TP53 gene replacement, *Cancer Res.* 63 (2003) 2737–2741.
- [20] K.E. Knudsen, D. Booth, S. Naderi, Z. Sever-Chroneos, A.F. Fribourg, C. Hunton, J.R. Feramisco, J.Y.J. Wang, E.S. Knudsen, RB-dependent S-phase response to DNA damage, *Mol. Cell. Biol.* 20 (2000) 7751–7763.
- [21] M. Hollstein, M. Hergenhahn, Q. Yang, H. Bartsch, Z.Q. Wang, P. Hainaut, New approaches to understanding p53 gene tumor mutation spectra, *Mutat. Res.* 431 (1999) 199–209.
- [22] M. Kaghad, H. Bonnet, A. Yang, L. Creancier, J.C. Biscan, A. Valent, A. Minty, P. Chalon, J.M. Lelias, X. Dumont, P. Ferrara, F. McKeon, D. Caput, Monoallelically expressed gene related to p53 at 1p36, a region frequently deleted in neuroblastoma and other human cancers, *Cell* 90 (1997) 809–819.
- [23] M.E. Lomax, D.M. Barnes, T.R. Hupp, S.M. Pickley, R.S. Camplejohn, Characterization of p53 oligomerization domain mutations isolated from Li-Fraumeni and Li-Fraumeni like family members, *Oncogene* 17 (1998) 643–649.
- [24] J.C. Bourdon, K. Fernandes, F. Murray-Zmijewski, G. Liu, A. Diot, D.P. Xirodimas, M.K. Saville, D.L. Lane, p53 isoforms can regulate p53 transcriptional activity, *Genes Dev.* 19 (2005) 2122–2137.
- [25] D. Goldschneider, E. Horvilleur, L.F. Plassa, M. Guillaud-Bataille, K. Million, E. Wittmer-Dupret, G. Danglot, H. de The, J. Benard, E. May, S. Douc-Rasy, Expression of C-terminal deleted p53 isoforms in neuroblastoma, *Nucleic Acids Res.* 34 (2006) 5603–5612.
- [26] N. Arai, D. Nomura, K. Yokota, D. Wolf, E. Brill, O. Shohat, V. Rotter, Immunologically distinct p53 molecules generated by alternative splicing, *Mol. Cell. Biol.* 6 (1986) 3232–3239.

Relationship of *DDX1* and *NAG* gene amplification/overexpression to the prognosis of patients with *MYCN*-amplified neuroblastoma

Setsuko Kaneko · Miki Ohira · Yohko Nakamura · Eriko Isogai · Akira Nakagawara · Michio Kaneko

Received: 14 June 2006 / Accepted: 28 August 2006 / Published online: 7 October 2006
© Springer-Verlag 2006

Abstract

Purpose Amplification of the *MYCN* gene strongly correlates with advanced stage, rapid tumor progression and poor prognosis in neuroblastoma (NB). Several genes in the *MYCN* amplicon, including the DEAD box polypeptide 1 (*DDX1*) gene, and neuroblastoma-amplified gene (*NAG* gene), have been found to be frequently co-amplified with *MYCN* in NB. The aim of this study was to clarify the prognostic significance of the co-amplification or overexpression of *DDX1* and *NAG* with *MYCN*.

Procedure The gene copy numbers and mRNA expression levels of *MYCN*, *DDX1*, and *NAG* in 113 primary NBs were determined by the real-time quantitative polymerase chain reaction or quantitative reverse transcriptase/polymerase chain reaction assay. The relationships between gene co-amplification/overexpression status and stage, age at diagnosis, and overall survival were analyzed.

Results For evaluating the frequency of *DDX1* and *NAG* co-amplification, it proved appropriate to discriminate NBs with <40 copies of *MYCN* amplification from those with ≥ 40 copies of *MYCN* (*DDX1*, $p = 0.00058$; *NAG*, $p = 0.0242$, χ^2 for independence test). In patients with *MYCN*-amplified NB aged ≥ 18 months, those with

tumor with enhanced *DDX1* expression and low-*NAG* expression showed a significantly better outcome than those with low-*DDX1* expression or enhanced *NAG* expression ($p = 0.0245$, log-rank test). None of the gene expression statuses had a significant relation to disease stage or survival for patients <18 months old. No relationship between any gene co-amplification status and disease stage, age at diagnosis, or overall survival was found.

Conclusions Our findings suggest that there may be a subset of NB in which enhanced *DDX1* and low-*NAG* expression consequent to *DDX1* co-amplification without *NAG* amplification contributes to susceptibility to intensive therapy. A larger study using an age cut-off of 18 months will be required.

Keywords Neuroblastoma · *MYCN* · *DDX1* · *NAG*

Abbreviations

NB	Neuroblastoma
<i>DDX1</i>	DEAD box polypeptide 1 gene
<i>NAG</i>	Neuroblastoma-amplified gene
hnRNP K	Heterogeneous nuclear ribonucleoprotein K
q-PCR	Quantitative polymerase chain reaction
q-RT-PCR	Quantitative reverse transcriptase/polymerase chain reaction
<i>BCM</i>	B-cell maturation factor gene
GAPDH	Glyceraldehyde 3-phosphate dehydrogenase

Introduction

Neuroblastoma (NB) is one of the most common malignant solid tumors in childhood. It presents with

S. Kaneko (✉) · M. Kaneko
Department of Pediatric Surgery,
Institute of Clinical Medicine,
University of Tsukuba,
Ibaraki 305-8575, Japan
e-mail: mkaneko@md.tsukuba.ac.jp

M. Ohira · Y. Nakamura · E. Isogai · A. Nakagawara
Division of Biochemistry,
Chiba Cancer Center Research Institute,
Chiba 260-8717, Japan

wide aggression from spontaneous regression or tumor maturation to rapid progression and fatality in most metastatic tumors diagnosed in children more than 1 year old. *MYCN* amplification occurs in about 25% of NB and is one of the most important markers in determining the aggressiveness of NB. Amplification of *MYCN* strongly correlates with advanced disease stage, rapid tumor progression and poor prognosis (Brodeur et al. 1984; Seeger et al. 1985; Brodeur and Seeger 1986). The size of the *MYCN* amplicon can span from 100 to 1,500 kb (Amler and Schwab 1989). Consequently, it is possible to suggest that additional genes being present in the amplicon and co-amplified with *MYCN* may contribute to the tumor phenotype. So far, several genes including the *DDX1* (DEAD box polypeptide 1) gene and *NAG* (NB-amplified gene) gene have been found to be frequently co-amplified with *MYCN* in NB (Beheshti et al. 2003; Scott et al. 2003a).

The *DDX1* is one of a family of genes that encode DEAD (asp-glu-ala-asp) box proteins. This gene maps to chromosome band 2p24 and 340 kb 5' of *MYCN* (Godbout and Squire 1993; Kuroda et al. 1996). Proteins with the DEAD box motif are putative ATP-dependent RNA helicases and more than 30 proteins have been identified from bacteria to humans (De Valoir et al. 1991; Kitajima et al. 1994). By altering the RNA secondary structure, they are implicated in diverse cellular processes such as RNA splicing, ribosome assembly, and translation initiation (Tanner and Linder 2001). Some members of the family are differentially expressed during embryogenesis, cellular growth, and division (Schmid and Linder 1992; Iost and Dreyfus 1994; Godbout et al. 2002). The biological function of *DDX1* remains unknown. In recent studies, *DDX1* was found to associate with factors involved in 3'-end cleavage and polyadenylation of pre-mRNAs (Bleoo et al. 2001). *DDX1* was also shown to have protein-protein interaction with heterogeneous nuclear ribonucleoprotein K (hnRNP K), and to have poly(A) RNA binding activity (Chen et al. 2002).

The *DDX1* gene has been known to be co-amplified with *MYCN* in 40–70% of NBs. There are reports showing a trend toward a worse clinical outcome with *MYCN* and *DDX1* co-amplification (Squire et al. 1995; George et al. 1997). Others have reported no significant difference in the clinical outcome or survival between patients with or without *DDX1* co-amplification (Manohar et al. 1995; De Preter et al. 2002). In a recent study of 98 *MYCN*-amplified NBs, a significant correlation of *DDX1* co-amplification with a better prognosis and improved patient survival was

shown by using semiquantitative multiplex PCR (Weber et al. 2004). In contrast to the observations by Weber et al., De Preter et al. have concluded that *DDX1* co-amplification had no significant prognostic value in *MYCN*-amplified tumors by re-evaluating their data (De Preter et al. 2005). The prognostic significance of *MYCN* and *DDX1* co-amplification has not been determined.

Recently, Scott et al. reported that the 5' end of *NAG* is located 30 kb telomeric to *DDX1*, with the two genes lying in opposite orientations (Scott et al. 2003b). They found a significant association between low-disease stage in *MYCN*-amplified tumors and *NAG* co-amplification. The function of *NAG* is as yet unclear.

To date, there have been no reports of measuring and analyzing accurate copy numbers and precise mRNA expression levels of *MYCN*, *DDX1*, and *NAG* genes in NB. In order to clarify the prognostic significance of the co-amplification or gene expression of *DDX1* and *NAG* with *MYCN*, we determined gene copy numbers and mRNA expression levels of *MYCN*, *DDX1*, and *NAG* genes in 113 primary NBs using the real-time quantitative polymerase chain reaction (q-PCR) or quantitative reverse transcriptase/polymerase chain reaction (q-RT-PCR) assay. The results were analyzed in relation to stage, age at diagnosis and overall survival.

Materials and methods

Tumor samples

One hundred and thirteen primary NBs were obtained from the Department of Pediatric Surgery, University of Tsukuba, and the Division of Biochemistry, Chiba Cancer Center Research Institute, Japan. Tumors detected by mass screening were excluded. Patients were aged between 0 months and 14 years at diagnosis (median 18 months). All 52 nonsurvivors died of progressive disease, while 59 of 61 survivors are free of the disease.

Tumors with the haploid *MYCN* gene copy number of more than five and less than two by the q-PCR assay were considered as *MYCN* amplified and unamplified, respectively.

DNA or RNA extraction

Tumor DNA was isolated by proteinase K/SDS digestion followed by phenol-chloroform extraction according to the standard protocol. DNA from human

placenta and a NB cell line CHP 134 were used as templates for the reference B-cell maturation factor (*BCM*) gene and test genes, respectively. The CHP 134 cell was found to have multiple copies of *MYCN*, *DDX1*, and *NAG* genes by preliminary q-PCR.

Total RNA was prepared from frozen tumor tissue according to the Acid Guanidinium–Phenol–Chloroform method (Chomczynski and Sacchi 1987). One microgram of each RNA was incubated with random primers and Superscript II reverse transcriptase (Invitrogen, Carlsbad, CA, USA) to yield cDNA.

Real-time q-PCR

Real-time q-PCR was carried out using the ABI Prism 7700 Sequence Detection System (Applied Biosystems, Foster City, CA, USA) as described by De Preter et al. with modification (De Preter et al. 2002). For quantification of the gene copy number, TaqMan probe assay was performed. The nucleotide sequences of the primers used are *MYCN*-f 5'-CGCAAAGCCACCTCTCATTA-3' and *MYCN*-r 5'-TCCAGCAGATGCCACATAAGG-3', *DDX1*-f 5'-TAGGAGGAGGTGATGTACTTATGGTAA-3' and *DDX1*-r 5'-AGCCTATGCAATTCTTAGAGTGTGT-3', *NAG*-f 5'-GACCAAGAAGTCTTTCCCTGC-3' and *NAG*-r 5'-GGTCAACAATACGTGGATAGAAGG-3', and *BCM*-f 5'-CGACTCTGACCATTGCTTTCC-3' and *BCM*-r 5'-AAGCAGCTGGCAGGCTCTT-3'.

The sequences of the TaqMan probes are *MYCN* 5'-FAM-TTCTGTAAATACCAATGACACATCCGCCTT-TAMRA-3', *DDX1* 5'-FAM-CCCAGCTACC AATCACCTCACCAAATT-TAMRA-3', *NAG* 5'-FAM-CAAGCTGCTGGTGAAGTGTGTCTCCA-TAMRA-3' and *BCM* 5'-FAM-CAACCATTCTTGTCACCACGAAAACGAA-TAMRA-3'. Twenty microliter of PCR reaction mixture for copy number determination consisted of template DNA, 1× q-PCR Mastermix (EUROGENTEC, Liege, Belgium), 300 nM of each primer and 200 nM of TaqMan probe. *MYCN*, *DDX1* or *NAG* gene assay was performed containing no-template control, standard CHP 134 DNA of five serial tenfold dilutions ranging from 100 ng to 10 pg, 10 ng of human placental DNA as a calibrator and ~10 ng of tumor DNA. The reference *BCM* gene assay included no-template control, standard human placental DNA of four serial tenfold dilutions ranging from 200 to 0.2 ng, 10 ng of human placental DNA as a calibrator and ~10 ng of tumor DNA. *BCM* gene is mapped to 16p13.1 and is located in a chromosomal region that rarely shows genetic abnormality (Vandesompele et al. 2001). Experiments were carried out in triplicate. The thermal cycling conditions for q-PCR

and q-RT-PCR were: 50°C for 2 min, 95°C for 10 min, 45 cycles at 95°C for 15 s and 60°C for 1 min.

Real-time q-RT-PCR

Expression levels of *MYCN*, *DDX1*, and *NAG* genes were measured in cDNA by the ABI Prism 7700 Sequence Detection System (Applied Biosystems). Human glyceraldehyde 3-phosphate dehydrogenase (*GAPDH*) was used as an internal control gene. cDNA from one of the 113 samples examined was used as the standard template because of its appropriate expression levels of *MYCN*, *DDX1*, *NAG*, and *GAPDH* mRNA by preliminary q-RT-PCR. The specific primers used are *MYCN*-f 5'-CACAAAGGCCCTCAGTACCTC-3' and *MYCN*-r 5'-CAGTGACCACGTCGATTTCTT-3', *DDX1*-f 5'-TGGAAGAGATGGATTGGCTC-3' and *DDX1*-r 5'-CCTGTTTCTGCAGCCATAAGTAC-3', *NAG*-f 5'-CAAATCACGGCAGTCACTACG-3' and *NAG*-r 5'-ACACACTTCACCA GCAGCTTG-3', and *GAPDH*-f 5'-GAAGGTGAA GGTCGGAGTC-3' and *GAPDH*-r 5'-GAAGATGG TGATGGGATTTTC-3'. The sequences of the TaqMan probes are *MYCN* 5'-FAM-AGAGGACACCCTGAGCGATTTCAGATG-TAMRA-3', *DDX1* 5'-FAM-CAACTGATATCCAGGCTGAATCTATCCCA-TAMRA-3', *NAG* 5'-FAM-TGTGACCAAGAACTTCTTTCCCTGCTCCT-TAMRA-3' and *GAPDH* 5'-FAM-CAAGCTTCCCGTTCTCAGCC-TAMRA-3'. The primers and probes were designed to be located on exons 2–3 for *MYCN* mRNA, exons 2–4 for *DDX1* mRNA, exons 51–52 for *NAG* mRNA, and exons 4–6 for *GAPDH* mRNA.

Twenty microliter of the PCR reaction mixture for quantification contained template cDNA, 1× qPCR Mastermix (EUROGENTEC), 300 nM of each primer and 200 nM of TaqMan probe. Each assay consisted of no-template control, standard cDNA of five serial tenfold dilutions ranging from 1 µg to 0.1 ng, and ~5 ng of tumor cDNA.

Statistical analysis

The relation of *DDX1* or *NAG* gene amplification to *MYCN* gene copy number was tested using χ^2 for an independence test. Correlations between the gene amplification/expression status and disease stage or age at diagnosis were compared by χ^2 for an independence test or Fisher's exact probability test. Mann–Whitney's *U*-test was used to evaluate the relationship between the gene expression level in tumors with or without gene amplification. Survival analysis was performed according to the Kaplan–Meier method and the log-rank test.

Results

The haploid *MYCN*, *DDXI*, and *NAG* gene copy number

Seventy-two of 113 tumors examined had *MYCN* amplification. Forty-one tumors were *MYCN*-unamplified; 17 in stages 1, 2 or 4s, nine in stage 3, and 15 in stage 4. Twenty-five and 16 patients were aged <18 and \geq 18 months at diagnosis, respectively. Seven of 41 patients died of disease, while all 34 survivors are free of disease. Patients with *MYCN*-amplified NB included four with stage 1, two with stage 2, two with stage 4s, 12 with stage 3, and 52 patients with stage 4 disease. Of 72 patients with *MYCN*-amplified tumor, 45 patients died of disease, while 25 of 27 survivors are free of disease. The follow-up period for *MYCN*-amplified survivors ranged from 17 to 93 months.

In 72 *MYCN*-amplified NBs, *DDXI*, and *NAG* genes were found to be co-amplified in 49 (68.1%) and 19 (26.4%) tumors, respectively (Fig. 1a, b). All 19 tumors with *NAG* amplification had also *DDXI* amplification. Forty-one tumors without *MYCN* amplification were unamplified for *DDXI* and *NAG*. By plotting precise gene copy numbers of *MYCN* and *DDXI*, and *MYCN* and *NAG* of each tumor on the same graphs, we found for the first time that NB with lower copies of *MYCN* amplification tended to a more frequent *DDXI* and *NAG* co-amplification than those with higher copies of *MYCN*. For evaluating the frequency of *DDXI* and *NAG* co-amplification, it proved appropriate to discriminate NBs with <40 copies of *MYCN* amplification from those with \geq 40 copies of *MYCN* (*DDXI*, $p = 0.00058$; *NAG*, $p = 0.0242$, χ^2 for independence test) (Fig. 1a, b).

Overall survival of patients with *MYCN*-amplified NB with or without *DDXI* and *NAG* co-amplification

For the 72 patients with *MYCN*-amplified NB, no statistically significant difference in survival probability was found among three gene co-amplification statuses, patients with tumor with *MYCN* amplification alone (*MYCN* alone), those with *DDXI* co-amplification alone (*MYCN* + *DDXI*), and those with both *DDXI* and *NAG* co-amplification (*MYCN* + *DDXI* + *NAG*) (*MYCN* alone versus *MYCN* + *DDXI*, $p = 0.465$; *MYCN* alone versus *MYCN* + *DDXI* + *NAG*, $p = 0.719$; *MYCN* + *DDXI* versus *MYCN* + *DDXI* + *NAG*, $p = 0.148$, log-rank test) (Fig. 2). We found no significant difference in overall survival between patients with tumor with *MYCN* amplification alone and those with *DDXI*-co-amplified NB regardless of *NAG* co-amplification ($p = 0.763$, log-rank test).

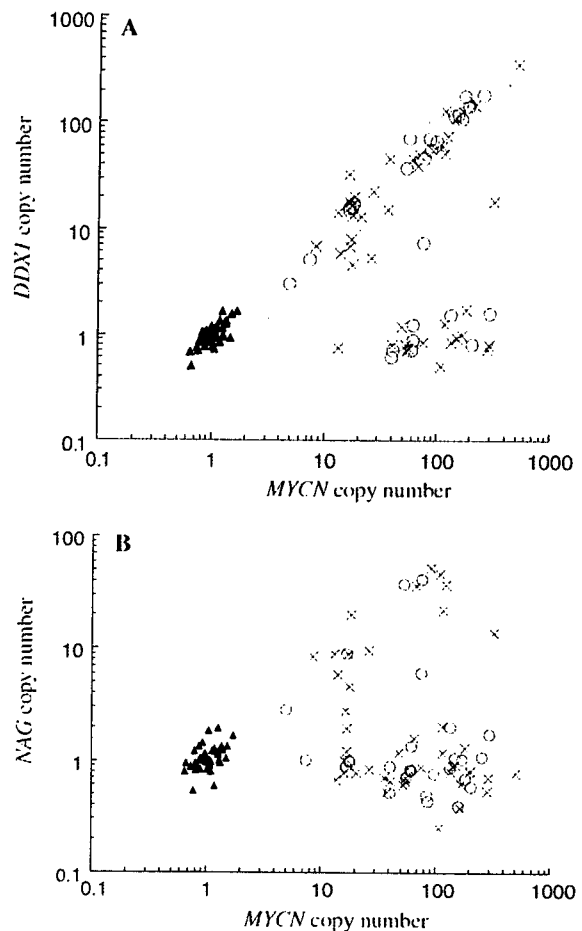


Fig. 1 The haploid *MYCN* and *DDXI* gene copy numbers (a), and *MYCN* and *NAG* gene copy numbers (b) in 113 NBs were determined by real-time q-PCR. Open circle, survivors with *MYCN* amplification ($n = 27$); cross, nonsurvivors with *MYCN* amplification ($n = 45$); filled triangle, patients without *MYCN* amplification ($n = 41$)

Relation of gene co-amplification status to disease stage or age at diagnosis

Table 1 shows the gene co-amplification status, disease stage and age at diagnosis of 72 patients with *MYCN*-amplified NB. Recently, an age cut-off higher than 12 months has been proposed as a prognostic predictor for comparison of survival rate in NB, suggesting an appropriate age cut-off of 18 months (London et al. 2005).

None of the gene co-amplification statuses had a significant correlation with disease stage (stages 1, 2, 3, and 4s versus stage 4) or age at diagnosis (<18 months versus \geq 18 months) (data not shown), with the exception of *NAG*, which tended toward a more frequent co-amplification with *MYCN* in stage 4 (17/52, 32.7%)

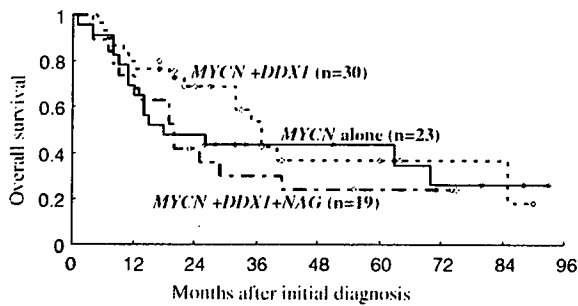


Fig. 2 Overall survival for patients with *MYCN*-amplified NB with or without *DDX1* and *NAG* co-amplification. No statistically significant difference in survival probability was found among three gene co-amplification statuses (*MYCN* alone versus *MYCN* + *DDX1*, $p = 0.465$; *MYCN* alone versus *MYCN* + *DDX1* + *NAG*, $p = 0.719$; *MYCN* + *DDX1* versus *MYCN* + *DDX1* + *NAG*, $p = 0.148$, log-rank test)

Table 1 Gene co-amplification status, disease stage and age at diagnosis of 72 patients with *MYCN*-amplified NB. There was no significant correlation between any gene co-amplification status and disease stage (stages 1, 2, 3, and 4s versus stage 4) or age at diagnosis among 72 patients with *MYCN*-amplified NB, with the exception of *NAG*, which tended toward a more frequent co-amplification with *MYCN* in stage 4 compared with stages 1, 2, 3, and 4s ($p = 0.0504$, χ^2 for independence test)

	Stage			Age (months)	
	1, 2 and 4s	3	4	<18	≥18
<i>MYCN</i> alone	4	4	15	10	13
<i>MYCN</i> + <i>DDX1</i>	4	6	20	11	19
<i>MYCN</i> + <i>DDX1</i> + <i>NAG</i>	0	2	17	10	9
Total	8	12	52	31	41

compared with stages 1, 2, 3, and 4s (2/20, 10.0%) ($p = 0.0504$, χ^2 for independence test).

The expression level of *MYCN*, *DDX1*, and *NAG*

We determined the precise expression levels of *MYCN*, *DDX1*, and *NAG* in 108 of 113 NBs. Sixty-seven of 108 tumors had *MYCN* amplification. The *MYCN*-amplified tumors had a significantly higher expression level of *MYCN* compared with *MYCN*-unamplified tumors ($p = 8.22 \times 10^{-15}$, Mann-Whitney's *U*-test). None of the *MYCN*-unamplified tumors showed an overexpression of *MYCN*, *DDX1*, and *NAG* (data not shown). We classified *DDX1* or *NAG* gene expression levels higher than the highest in *MYCN*-unamplified tumors as enhanced.

In general, *DDX1* expression increased according to the *DDX1* copy number (Fig. 3a). The expression level of *DDX1* in tumors with *MYCN* amplification alone

was as low as that without *MYCN* amplification. Enhanced *DDX1* expression had no significant correlation with prognosis ($p = 0.925$, log-rank test).

The expression level of *NAG* in *NAG* co-amplified tumors was significantly higher than that in tumors without *NAG* co-amplification ($p = 5.77 \times 10^{-6}$, Mann-Whitney's *U*-test); however, *NAG* amplification was not necessarily accompanied with enhanced *NAG* expression (Fig. 3b). Enhanced *NAG* expression had no significant relation to disease stage (stage 1, 2, 3, and 4s versus stage 4) ($p = 0.462$, Fisher's exact probability test) or clinical outcome ($p = 0.0915$, log-rank test).

Relation of *DDX1* and *NAG* gene expression statuses to survival probability for patients with *MYCN*-amplified NB

None of the gene expression statuses had a significant correlation with disease stage and with survival for patients aged <18 months (data not shown).

In 41 patients with *MYCN*-amplified NB aged ≥18 months, those with tumor with enhanced *DDX1* expression and low-*NAG* expression had a significantly better outcome than those with low-*DDX1* expression or enhanced *NAG* expression ($p = 0.0245$, log-rank test) (Fig. 4a, b). The 16 tumors with enhanced *DDX1* and low-*NAG* expression included one with stage 2, four with stage 3, and 11 tumors with stage 4. All 16 tumors had *MYCN* and *DDX1* co-amplification without *NAG* amplification.

Discussion

Amplification of the *MYCN* gene is strongly associated with the rapid progression of NB and advanced disease stage (Brodeur et al. 1984; Seeger et al. 1985). The prognosis of patients with stage 4 tumors with *MYCN* amplification had been extremely poor. In 1999, Kaneko et al. reported treatment results with improved survival rate of patients with advanced NB aged 1 year or older treated with an intensive induction and consolidation chemotherapy regimens (Kaneko et al. 1999). With the use of a more intensive induction regimen followed by hematopoietic stem cell transplantation for *MYCN*-amplified stage 4 patients, survival curves for those with or without *MYCN* amplification appeared similar. In other words, the prognosis of patients with stage 4 NB without *MYCN* amplification remained poor (Kaneko et al. 2002). Their assessment of *MYCN* amplification status was based on the Southern blot technique. Measuring an accurate *MYCN* copy number in tumors is essential in

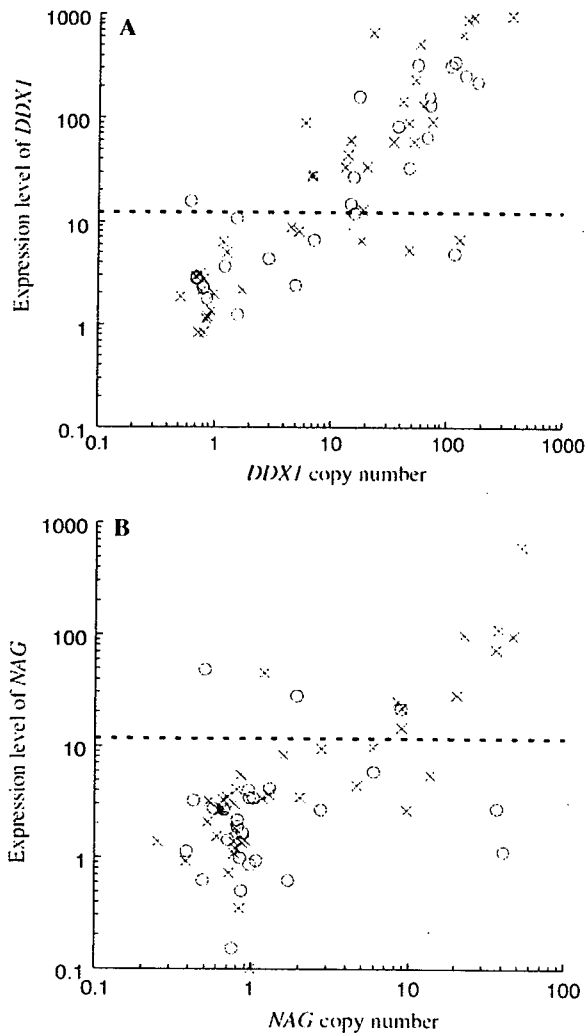


Fig. 3 Gene copy number and gene expression level of *DDX1* (a) and *NAG* (b) in 67 *MYCN*-amplified NBs. Open circle, survivors with *MYCN* amplification ($n = 26$); cross, nonsurvivors with *MYCN* amplification ($n = 41$); dotted line, the highest expression level of *DDX1* (a) or *NAG* (b) in *MYCN*-unamplified NBs

order to select the optimal treatment and improve survival for patients with advanced NB. Assays for the rapid and accurate quantification of *MYCN* copy number and *MYCN* expression level in NB have been developed by real-time q-PCR or q-RT-PCR method with TaqMan probe (Raggi et al. 1999; Tajiri et al. 2001; De Preter et al. 2002). Tanaka et al. reported that in their highly sensitive analysis by a q-PCR method combined with FISH, cases with more than two *MYCN* gene dosages ($MYCN/p53 \geq 2.0$) were significantly associated with unfavorable prognostic factors (Tanaka et al. 2004). In our study, we did not investigate NBs with a haploid *MYCN* gene copy number of between two and five.

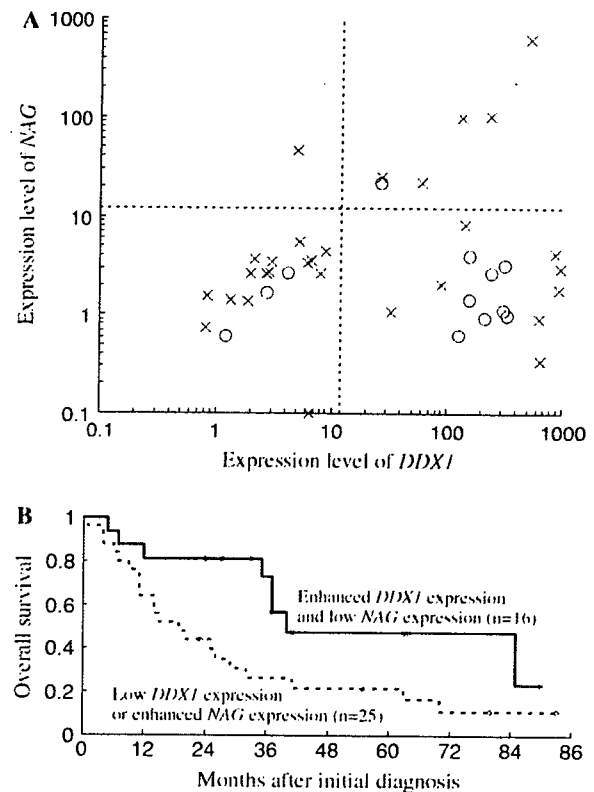


Fig. 4 a Expression level of *DDX1* and *NAG* mRNA in 41 *MYCN*-amplified NBs from patients aged ≥ 18 months. Open circle, survivors with *MYCN* amplification ($n = 12$); cross, nonsurvivors with *MYCN* amplification ($n = 29$); dotted lines, the highest expression levels of *DDX1* and *NAG* in *MYCN*-unamplified NBs. b In the 41 patients with *MYCN*-amplified NB aged ≥ 18 months, those with tumor with enhanced *DDX1* expression and low-*NAG* expression showed a significantly better outcome than those with low-*DDX1* expression or enhanced *NAG* expression ($p = 0.0245$, log-rank test)

Recently, Scott et al. found that the 7.3 kb transcript of the *NAG* gene with 52 exons, which is predominantly expressed in NB, covers 420 kb of genomic DNA. They proposed that probes for Southern blot or FISH studies, or primers used for PCR-based methods, should include the 3' end of the *NAG* gene over 400 kb away from *DDX1* (Scott et al. 2003b). The primers and TaqMan probe we designed were located on the 3' end of the *NAG* gene, on exon 52, and the frequency of *NAG* co-amplification with *MYCN* was in accordance with that reported by Scott et al.

It is thought that a low copy number of *MYCN* in *MYCN*-amplified human NB cells is correlated with a low degree of recombination and large amplicon size (Amler and Schwab 1989). Consistent with the findings by Amler and Schwab, we found for the first time that NB with lower copies of *MYCN* amplification tended

to a more frequent *DDX1* and *NAG* co-amplification than those with higher copies of *MYCN*. For evaluating the frequency of *DDX1* and *NAG* co-amplification, it proved appropriate to discriminate NBs with <40 copies of *MYCN* amplification from those with ≥ 40 copies of *MYCN*. The information obtained from these observations may be different from a recent suggestion by De Preter et al. that the process of co-amplification within the *MYCN* amplicon occurs coincidentally, and is not subject to selection (De Preter et al. 2005).

The prognostic significance of *DDX1* co-amplification with *MYCN* has remained unclear. Squire et al. analyzed 13 *MYCN*-amplified patients and showed a trend toward a worse clinical outcome with *DDX1* co-amplification (Squire et al. 1995). George et al. reported that with the exclusion of patients with 4S disease, those with *DDX1* co-amplification had a significantly shorter mean disease-free interval compared with *MYCN* amplification alone (George et al. 1997). However, they described that there was no significant difference in the proportion of survivors in these two groups. In contrast, Weber et al. reported that *DDX1* co-amplification correlated with an improved patient survival in 98 *MYCN*-amplified NB (Weber et al. 2004). In our study of 72 patients with *MYCN*-amplified NB, there was no significant difference in survival probability between patients with *DDX1*-co-amplified NB and those with tumor with *MYCN* amplification alone. The result was similar to those reported by Manohar et al. and De Preter et al. (Manohar et al. 1995; De Preter et al. 2002, 2005).

The *NAG* tended toward a more frequent co-amplification with *MYCN* in stage 4 compared with other stages, in contrast to the result of a significant association of *NAG* co-amplification with low-stage disease by Scott et al. (2003b). The difference was probably caused by the lower frequency of *NAG* co-amplification with *MYCN*. Amplification of *NAG* was not necessarily accompanied with enhanced *NAG* expression, and *NAG* expression level in *MYCN*-amplified tumors showed no significant relation to disease stage. The relationship between RNA expression levels of *DDX1* or *NAG* and clinical outcome for patients with *MYCN*-amplified NB has hardly been studied. Weber et al. reported that a high expression level of *DDX1* was associated with a trend toward a better survival probability while *NAG* expression was not correlated with prognosis (Weber et al. 2004). They drew the result using RNAs from 19 *MYCN*-amplified NB samples. We analyzed *DDX1* and *NAG* gene expression in 67 *MYCN*-amplified NB. Enhanced *DDX1* and *NAG* expression had no significant correlation with prognosis, respectively.

For the discrimination of prognosis for patients with NB, an age cut-off of 12 months was adopted worldwide. However, the International Neuroblastoma Pathology Classification, established for the prognostic evaluation of patients with neuroblastic tumors, has incorporated age factor of 18 months in the system (Shimada et al. 2001; Sano et al. 2006). The Children's Cancer Group in the USA has already chosen the 18 months as an age cut-off (Schmidt et al. 2005). Recent evidence supports the age cut-off ranging 15–18 months based on the results from the German analysis and two Children's Oncology Group analyses (London et al. 2005). In our study, the *DDX1* and *NAG* gene expression status in *MYCN*-amplified NBs revealed an age cut-off of 18 months to be an appropriate prognostic predictor of survival. We found that older patients with enhanced *DDX1* expression and low-*NAG* expression had a significantly better prognosis than those with low-*DDX1* expression or enhanced *NAG* expression. These findings indicate that, for *MYCN*-amplified NB from patients aged ≥ 18 months, both enhanced *DDX1* expression and low-*NAG* expression may be associated with a better response to intensive therapy. It is also possible to suggest a subset of NB in which enhanced *DDX1* and low-*NAG* expression consequent to *MYCN* and *DDX1* co-amplification without *NAG* amplification contributes to patient survival.

A larger cohort of patients and longer follow-up period using an age cut-off of 18 months will be required to clarify the clinical and prognostic significance of the expression status of both *DDX1* and *NAG* genes with *MYCN*.

References

- Amler LC, Schwab M (1989) Amplified N-myc in human neuroblastoma cells is often arranged as clustered tandem repeats of differently recombined DNA. *Mol Cell Biol* 9:4903–4913
- Beheshti B, Braude I, Marrano P, Thorner P, Zielenska M, Squire JA (2003) Chromosomal localization of DNA amplifications in neuroblastoma tumors using cDNA microarray comparative genomic hybridization. *Neoplasia* 5:53–62
- Bleoo S, Sun X, Hendzel MJ, Rowe JM, Packer M, Godbout R (2001) Association of human DEAD box protein DDX1 with a cleavage stimulation factor involved in 3'-end processing of pre-mRNA. *Mol Biol Cell* 12:3046–3059
- Brodeur GM, Seeger RC, Schwab M, Varmus HE, Bishop JM (1984) Amplification of N-myc in untreated human neuroblastoma correlates with advanced disease stage. *Science* 224:1121–1124
- Brodeur GM, Seeger RC (1986) Gene amplification in human neuroblastoma: basic mechanisms and clinical implications. *Cancer Genet Cytogenet* 19:101–111
- Chen HC, Lin WC, Tsay YG, Lee SC, Chang CJ (2002) An RNA helicase, DDX1, interacting with poly(A) RNA and hetero-

- geneous nuclear ribonucleoprotein K. *J Biol Chem* 277:40403–40409
- Chomczynski P, Sacchi N (1987) Single-step method of RNA isolation by acid guanidinium thiocyanate-phenol-chloroform extraction. *Anal Biochem* 162:156–159
- De Preter K, Spelemam F, Combaret V, Lunec J, Laureys G, Eussen BH, Francotte N, Board J, Pearson AD, De Paepe A, Van Roy N, Vandesompele J (2002) Quantification of MYCN, DDX1, and NAG gene copy number in neuroblastoma using a real-time quantitative PCR assay. *Mod Pathol* 15:159–166
- De Preter K, Spelemam F, Combaret V, Lunec J, Board J, Pearson A, De Paepe A, Van Roy N, Laureys G, Vandesompele J (2005) No evidence for correlation of DDX1 gene amplification with improved survival probability in patients with MYCN-amplified neuroblastomas. *J Clin Oncol* 23:3167–3168
- De Valoir T, Tucker MA, Belikoff EJ, Camp LA, Bolduc C, Beckingham K (1991) A second maternally expressed Drosophila gene encodes a putative RNA helicase of the DEAD box family. *Proc Natl Acad Sci USA* 88:2113–2117
- George RE, Kenyon R, McGuckin AG, Kohl N, Kogner P, Christiansen H, Pearson AD, Lunec J (1997) Analysis of candidate gene co-amplification with MYCN in neuroblastoma. *Eur J Cancer* 33:2037–2042
- Godbout R, Squire JA (1993) Amplification of a DDX1 box protein gene in retinoblastoma cell lines. *Proc Natl Acad Sci USA* 90:7578–7582
- Godbout R, Packer M, Katyal S, Bleoo S (2002) Cloning and expression analysis of the chicken DEAD box gene DDX1. *Biochim Biophys Acta* 1574:63–71
- Iost I, Dreyfus M (1994) mRNAs can be stabilized by DEAD-box proteins. *Nature* 372:193–196
- Kaneko M, Tsuchida T, Uchino J, Takeda T, Iwafuchi M, Ohnuma N, Mugishima H, Yokoyama J, Nishihira H, Nakada K, Sasaki S, Sawada T, Kawa K, Nagahara N, Suita S, Sawaguchi S (1999) Treatment results of advanced neuroblastoma with the first Japanese Study Group Protocol. *J Pediatr Hematol Oncol* 21:190–197
- Kaneko M, Tsuchida T, Mugishima H, Ohnuma N, Yamamoto K, Kawa K, Iwafuchi M, Sawada T, Suita S (2002) Intensified chemotherapy increases the survival rates in patients with stage 4 neuroblastoma with MYCN amplification. *J Pediatr Hematol Oncol* 24:613–621
- Kitajima Y, Yatsuki H, Zhang R, Matsuhashi S, Hori K (1994) A novel human homolog of a DEAD-box RNA helicase family. *Biochem Biophys Res Commun* 199:748–754
- Kuroda H, White PS, Sulman EP, Manohar CF, Reiter JL, Cohn SL, Brodeur GM (1996) Physical mapping of the DDX1 gene to 340 kb 5' of MYCN. *Oncogene* 13:1561–1565
- London WB, Boni L, Simon T, Berthold F, Twist C, Schmidt ML, Castleberry RP, Matthay KK, Cohn SL, De Bernardi B (2005) The role of age in neuroblastoma risk stratification: the German, Italian, and children's oncology group perspectives. *Cancer Lett* 228:257–266
- Manohar CF, Salwen HR, Brodeur GM, Cohn SL (1995) Co-amplification and concomitant high levels of expression of a DEAD box gene with MYCN in human neuroblastoma. *Genes Chromosomes Cancer* 14:196–203
- Raggi CC, Bagnoni ML, Tonini GP, Maggi M, Vona G, Pinzani P, Mazzocco K, De Bernardi B, Pazzagli M, Orlando C (1999) Real-time quantitative PCR for the measurement of MYCN amplification in human neuroblastoma with the TaqMan detection system. *Clin Chem* 45:1918–1924
- Sano H, Bonadio J, Gerbing RB, London WB, Matthay KK, Lukens JN, Shimada H (2006) International neuroblastoma pathology classification adds independent prognostic information beyond the prognostic contribution of age. *Eur J Cancer* 42:1113–1119
- Schmid SR, Linder P (1992) D-E-A-D protein family of putative RNA helicases. *Mol Microbiol* 6:283–291
- Schmidt ML, Lal A, Seeger RC, Maris JM, Shimada H, O'Leary M, Gerbing RB, Matthay KK (2005) Favorable prognosis for patients 12 to 18 months of age with stage 4 nonamplified MYCN neuroblastoma: a Children's Cancer Group Study. *J Clin Oncol* 23:6474–6480
- Scott D, Elsdon J, Pearson A, Lunec J (2003a) Genes co-amplified with MYCN in neuroblastoma: silent passengers or co-determinants of phenotype? *Cancer Lett* 197:81–86
- Scott DK, Board JR, Lu X, Pearson AD, Kenyon RM, Lunec J (2003b) The neuroblastoma amplified gene, NAG: genomic structure and characterisation of the 7.3 kb transcript predominantly expressed in neuroblastoma. *Gene* 307:1–11
- Seeger RC, Brodeur GM, Sather H, Dalton A, Siegel SE, Wong KY, Hammond D (1985) Association of multiple copies of the N-myc oncogene with rapid progression of neuroblastomas. *N Engl J Med* 313:1111–1116
- Shimada H, Umehara S, Monobe Y, Hachitanda Y, Nakagawa A, Goto S, Gerbing RB, Stram DO, Lukens JN, Matthay KK (2001) International neuroblastoma pathology classification for prognostic evaluation of patients with peripheral neuroblastic tumors: a report from the Children's Cancer Group. *Cancer* 92:2451–2461
- Squire JA, Thorner PS, Weitzman S, Maggi JD, Dirks P, Doyle J, Hale M, Godbout R (1995) Co-amplification of MYCN and a DEAD box gene (DDX1) in primary neuroblastoma. *Oncogene* 10:1417–1422
- Tajiri T, Tanaka S, Shono K, Kinoshita Y, Fujii Y, Suita S, Ihara K, Hara T (2001) Quick quantitative analysis of gene dosages associated with prognosis in neuroblastoma. *Cancer Lett* 166:89–94
- Tanaka S, Tajiri T, Noguchi S, Shono K, Ihara K, Hara T, Suita S (2004) Clinical significance of a highly sensitive analysis for gene dosage and the expression level of MYCN in neuroblastoma. *J Pediatr Surg* 39:63–68
- Tanner NK, Linder P (2001) DExD/H box RNA helicases: from generic motors to specific dissociation functions. *Mol Cell* 8:251–262
- Vandesompele J, Speleman F, Van Roy N, Laureys G, Brinkschmidt C, Christiansen H, Lampert F, Lastowska M, Bown N, Pearson A, Nicholson JC, Ross F, Combaret V, Delattre O, Feuerstein BG, Plantaz D (2001) Multicentre analysis of patterns of DNA gains and losses in 204 neuroblastoma tumors: How many genetic subgroups are there? *Med Pediatr Oncol* 36:5–10
- Weber A, Imisch P, Bergmann E, Christiansen H (2004) Coamplification of DDX1 correlates with an improved survival probability in children with MYCN-amplified human neuroblastoma. *J Clin Oncol* 22:2681–2690